Fungal Ecology 72 (2024) 101385

Contents lists available at ScienceDirect

Fungal Ecology

journal homepage: www.elsevier.com/locate/funeco

Transcriptomic and protein analysis of *Trametes versicolor* interacting with a *Hypholoma fasciculare* mycelium foraging in soil

G. Attrill [a], L. Boddy [b], E. Dudley [c], B. Greenfield [a,d], D.C. Eastwood [a,*]

[a] Department of Biosciences, Singleton Park Campus, Swansea University, Swansea, SA2 8PP, United Kingdom
[b] School of Bioscience, Cardiff University, Cardiff, CF10 3AX, United Kingdom
[c] Faculty of Medicine, Health and Life Science, Swansea University, Singleton Park, Swansea, SA2 8PP, United Kingdom
[d] National Resources Wales, Maes Newydd, Llandarcy, Neath Port Talbot, SA10 6JQ, United Kingdom

ARTICLE INFO

Handling Editor: Prof. Benjamin E. Wolfe

ABSTRACT

The decomposition of large woody material is an important process in forest carbon cycling and nutrient release. Cord-forming saprotrophic basidiomycete fungi create non-resource limited mycelial networks between decomposing branches, logs and tree stumps on the forest floor where colonisation of new resources is often associated with the replacement of incumbent decay communities. To date, antagonism experiments have mostly placed competing fungi in direct contact, while in nature cord-forming saprobes encounter colonised wood as mycelia in a network. Transcriptomic and peptide analyses were conducted on soil-based microcosms were foraging cord-forming *Hypholoma fasciculare* encountered a wood block colonised by *Trametes versicolor*. Protein turnover featured strongly for both species and genes putatively involved in secondary metabolite production were identified. *H. fasciculare* demonstrated an exploitative profile with increased transcription of genes associated with carbohydrate metabolism and RNA and ribosome processing. *T. versicolor* showed a shift in signalling, energy generation and amino acid metabolism. By identifying genes and proteins putatively involved in this fungal interaction, this work may help guide the discovery of bioactive molecules and mechanisms underpinning community succession.

1. Introduction

Forests and woodlands play a major role in global terrestrial carbon cycling whereby atmospheric carbon fixation by photosynthesis is largely balanced by decomposition of an equivalent amount of dead material (Boddy and Watkinson, 1995; Baldrian 2008; Woodward and Boddy, 2008; Gessner et al., 2010; Ballasen and Luyssaert, 2014). This makes available again those mineral nutrients that had been 'locked up' in dead tissues. Wood is structurally and chemically complex, allowing only microbes with specific decay adaptations to use it as a source of nutrition. A narrow range of basidiomycetes and ascomycetes are the major agents of wood decomposition, by virtue of their mycelial nature and wide enzyme array allowing them to gain access to large pieces of organic matter (Tláskal et al., 2021). Although many of these species can decompose wood completely, in nature a succession of different species is usually involved, determined by time of arrival, antagonistic ability and tolerance of disturbance and stress (Boddy and Hiscox, 2016). In the absence of stress and disturbance, antagonism is the main driver of community change (Boddy, 2000; Boddy and Heilmann-Clausen, 2008; Boddy and Hiscox, 2016). The ultimate outcome of antagonistic interactions at the mycelial level is full, partial or reciprocal replacement, or deadlock where neither species acquires any of the opponent's territory (Boddy, 2000; Boddy and Hiscox 2016). These differences in outcomes are reflected in a hierarchy of competitive ability, some species being generally poor competitors and at the other extreme species outcompeting most (Holmer et al., 1997; Boddy, 2000; Boddy and Hiscox, 2016). The fungi involved in wood decay can be categorised crudely into three non-mutually exclusive categories according to the stage of decay in which they colonise the substrate, i.e. primary, secondary and tertiary colonisers, and in the absence of stress this is broadly correlated with competitive ability.

Antagonistic interactions occur at a distance or following contact (Rayner and Boddy, 1988; Boddy 2000, 2016). Although some contact antagonisms, e.g. mycoparasitism, are relatively subtle, the vast majority of antagonistic interactions involve the production of inhibitory volatiles (sesquiterpenes, ketones, alcohols and aromatics) and

* Corresponding author.
E-mail address: d.c.eastwood@swansea.ac.uk (D.C. Eastwood).

https://doi.org/10.1016/j.funeco.2024.101385
Received 13 October 2023; Received in revised form 29 August 2024; Accepted 5 September 2024
Available online 27 September 2024

diffusible organic compounds, such as enzymes, toxins and metabolites (Boddy 2000; Baldrian, 2004; Hynes et al., 2007; Evans et al., 2008, Hiscox et al., 2010a; Hiscox and Boddy 2017; Hiscox et al., 2018; O'Leary et al., 2019). Oxidative stress and production of reactive oxygen species are also commonly associated with antagonistic interactions (Tornberg and Olsson, 2002). Defence and repair chemicals are up-regulated (Hiscox et al., 2018), as are nutrition-linked enzymes, including β-glucosidase, acid phosphatase and chitinase (Reyes et al., 1990; Lindahl and Finlay, 2006). Also, agar studies have shown that the genes involved in cytokinesis and cell signalling are up-regulated (Eyre et al., 2010).

The availability of annotated genomes facilitates functional assessment of the underlying mechanisms of plant biomass decomposition by fungi. Transcriptomic and, increasingly, proteomic and metabolomic analyses have been used to investigate underpinning decay mechanisms expressed by fungi (Miyauchi et al., 2016; Hori et al., 2018; Peng et al., 2018; Sahu et al., 2020). Molecular responses of fungi to changes in abiotic conditions and to the substrate during decay progression continue to advance our understanding of decay processes (Chase, 2003; Presley and Schilling, 2017; Moody et al., 2018). Such transcriptomic and proteomic experiments to elucidate decay mechanisms have, however, typically been performed in fresh wood, irrespective of when a fungus colonises naturally. That is, transcriptomics and proteomics have rarely been investigated in the more natural situation where a fungus attempts to colonise wood pre-colonised by another fungal species.

Dead wood resources are distributed heterogeneously in space and time in the canopy, on the forest floor, and as dead woody roots below ground. Most fungi spread between resources as spores, their mycelia being restricted to the resource that they have colonised (termed resource-unit-restricted) (Hiscox and Boddy 2016). However, a few can grow out of resources as mycelium in search of new resources (termed non-resource-unit-restricted). The mycelia of non-resource-unit-restricted wood decay fungi have diffuse growth fronts that search for new resources but which, behind the front, tend to aggregate into cords of parallel-aligned multi-hyphal linear organs that form highly interconnected networks on the forest floor (Boddy 1999; Fricker et al. 2008, 2017). These cords are conduits through which water and nutrients can be translocated rapidly. Typically, such fungi are also highly antagonistic.

Assessing the mechanisms of protein synthesis and gene expression using an ecologically relevant experimental set-up will provide valuable insight into the specific responses to interspecific competition between two common wood decay species and wider consideration for succession and community development in forest floor fungal decomposition communities. In this study, we conducted a transcriptomic and peptide analysis of the replacement of *Trametes versicolor* (a resource-unit-restricted secondary coloniser) by *Hypholoma fasciculare* (a highly antagonistic, cord-forming tertiary coloniser) in soil microcosms. Wood blocks colonised separately by these species were well-separated, to mimic spatially separated resources in the natural environment. In this scenario the mycelial cord-forming *H. fasciculare* grew out of its resources and subsequently encountered a wood block colonised by *T versicolor*.

2. Methods

2.1. Fungal sample preparation and culturing

The genome-sequenced *Trametes versicolor* monokaryotic strain FP-101664 (Floudas et al., 2012) was used to generate stable dikaryotic strains with mycelial growth characteristics similar to the routinely used dikaryotic *T. versicolor* CCJH1 strain (Hiscox et al., 2010b, 2015). Several *T. versicolor* monokaryons were paired with the sequenced *T. versicolor* monokaryon. The mean colony diameter (n = 10) of the resulting dikaryons after 6 days (144 h post sub-culture) at 20 °C on 0.5% malt extract agar (MEA 5 gl^{-1} Munton and Fison malt, 15 gl^{-1} Lab M agar no.2) were compared (one-way ANOVA; Post-hoc Tukey 95%; Supplementary Table S1). The synthesised dikaryon (TvFPH) with greatest similarity to *T. versicolor* CCJH1, in terms of extension rate and colony morphology, was used for the remainder of this study.

Stock culture collection samples were stored on slopes of 2% MEA at 4 °C. Isolates were sub-cultured every 9 days from metabolically active colony margins and incubated in the dark at 20 °C. All isolates are available from the Cardiff University Culture Collection. *Hypholoma fasciculare* strain GTWV2 was used throughout the study, selected as an ecologically significant, highly antagonistic later decay stage coloniser that occupied the same habitats as *T. versicolor*. The *H. fasciculare* GTWV2 isolate spore culture was isolated from a fruit body, South Wales, UK, by G. Tordoff as part of the study Tordoff et al. (2008). While no annotated genome was available for *H. fasciculare* at the time of study, a fully annotated *Hypholoma sublateritium* sequence was through the JGI mycocosm platform. Although not ideal and potentially resulting in the loss of some *H. fasciculare* transcripts, the published *H. sublateritium* genome would allow differential comparison with the sequenced *T. versicolor*-derived transcripts. No alternative, ecologically appropriate, cord-forming, late stage decay fungus genome was available at the time of study.

Beech (*Fagus sylvatica*) wood blocks (2 cm × 2 cm x 1 cm height) were cut by Old Saw Mill Ltd (Newport, UK) from a freshly-felled mature beech tree supplied by Natural Resources Wales. Blocks were cut so that the wood vessels ran along the longest, 2 cm, axis. Wood blocks were autoclaved in three cycles at 121 °C for 30 min with 24 h intervals between each cycle and stored at −18 °C before being placed vessel downwards in direct contact *H. fasciculare* or *T. versicolor* 0.5% MEA cultures in triple vented 14 cm Petri dishes (Greiner Bio-one Austria). All cultures were sealed with Parafilm® and incubated in dark at 20 °C for 84 days as described in Hiscox et al. (2010a). Full colonisation of wood blocks at 84 days was confirmed by placing wood fragments from 5 sampling points in 5 chisel-split replicate wood blocks (Fig. 1) onto 2% MEA and checking for emergence of the appropriate fungus. Density of uncolonised wood blocks, and wood blocks colonised by *H. fasciculare* and *T. versicolor* after initial colonisation was determined as oven dry weight (at 80 °C) divided by fresh volume (cm^3; from Vernier calliper measurements).

2.2. Preparation of soil microcosms

Wood block-based interaction experiments between *H. fasciculare* and *T. versicolor* were conducted in soil microcosms using 24 × 24 cm bioassay dishes (Fig. 1). Unsterilized soil was used to better mimic the environment of the forest floor and provide an organic surface for mycelial cords to extend across. Loamy soil was collected at a depth of 25 cm from a deciduous woodland - Coed y Beddick in Tintern UK (NGR 352800, 201800, 51° 41′ 48.37″ N, 2° 40′ 53.11″ W), and roughly sieved (10 mm) on site. The soil was air dried in the laboratory, finely sieved (2 mm) and frozen at −18 °C for 48 h (to prevent population explosions of fungal-feeding collembola). Microcosms were prepared (following Crowther et al., 2011) by mixing 200 g of air dry soil with 340 ml of DH_2O to give a water potential of −0.012 kPa (determined by the method of Fawcett and Collis-George, 1967), and compressing evenly to a depth of 5 mm in plastic bio-assay dishes (24 × 24 cm).

Pre-colonised wood blocks were aseptically scraped free of surface mycelium and placed onto the microcosm soil surface so that relative positions were standardised between replicates (ten) and vessels orientated horizontally (Fig. 1). A block with *H. fasciculare* was placed 12.7 cm from a corner and the microcosms were stacked, loosely covered with black polythene bags and incubated at 20 °C with 70% relative humidity. A *T. versicolor* single species control microcosm was prepared by replacing the *H. fasciculare* inoculum with a *T. versicolor*-colonised wood block. Following *H. fasciculare* emergence from the wood block onto the microcosm soil (~5 days), a block of *T. versicolor* was added to the microcosms 12.7 cm to the diagonally opposite corner from the *H. fasciculare* block and incubation continued. *H. fasciculare* single

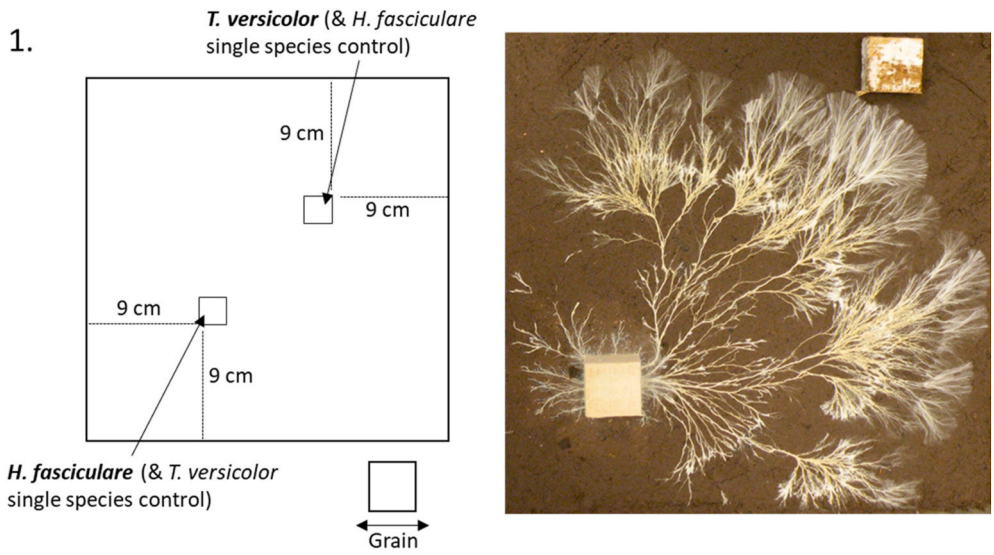

Fig. 1. Experimental design where 24 × 24 cm^2 soil-based microcosms were inoculated with wood blocks (2 cm length x 2 cm width x 1 cm height) colonised by the fungi as shown. Image shows the point at which *H. fasciculare* cords visibly met the *T. versicolor*-colonised wood block.

species control microcosms were prepared by replacing the *T. versicolor* block with one previously colonised by *H. fasciculare*. Microcosms were individually weighed before the experiment commenced and every 5 days after. Water content was maintained by gentle misting with appropriate weight of sterile DH_2O using a sterile atomiser.

2.2.1. Mycelial extension rate of H. fasciculare in microcosms

Mycelium emergence of the cord-forming *H. fasciculare* was assessed periodically to determine the time of contact with the second wood block for each replicate (circa 25 days). Foraging extension rate was determined by image analysis (IMAGEJ, National Institute of Health, USA) of photographs (Nikon Coolpix 57000 camera mounted 40 cm above each microcosm) taken at 5 d intervals. Following setting image parameters to 8-bit binary threshold, pixels containing mycelia and soil were highlighted red and black respectively. *H. fasciculare* mycelial cord extension rate (cm d^{-1}) was determined as the mean distance of mycelial extent measured along straight lines at 45°angle intervals from the centre of the initially colonised wood block over time (Crowther et al., 2011).

2.2.2. Wood decay rate in microcosms

A further ten replicates of each set of microcosms was incubated for an additional 85 d after others had been harvested for transcriptomic and peptide analysis. Density of wood blocks (single species controls, *H. fasciculare* inoculum and *H. fasciculare – T. versicolor* interaction) was then determined, as above, and decay rate estimated by comparison of density at harvest with density at the time of setting up the microcosms.

2.3. Transcriptomic and peptide analysis

2.3.1. Wood block sampling

For transcript and protein analysis experiments, colonised wood blocks were harvested 14 days after *H. fasciculare* cords visibly met the *T. versicolor* wood block to ensure sufficient time for antagonism between the interacting species. Blocks from interaction and single species microcosms were frozen immediately under liquid nitrogen, freeze dried and stored at −80 °C. Three replicates of each treatment were used for subsequent transcriptomic and peptide analysis. Wood decay rate (g cm^{-3} d^{-3}) was determined for both fungal species by comparing wood block density 84 days following *H. fasciculare* mycelial contact with wood blocks of each species harvested immediately prior to setting up the interaction experiments. Five replicates were used for each sample group.

2.3.2. RNA extraction for transcriptome analysis

Sawdust was collected from frozen wood blocks that had been clamped in a bench top vice and grated using a micro-plane and transferred to eight sterile RNase-free homogeniser tubes (Precellys®24, Bertin Instruments, France) placed in ice and containing 1 ml of Tris-EDTA buffer (10 mM Tris-HCl pH8 containing 1 mM EDTA, Na_2). Samples were disrupted in a Precellys®24 homogeniser set to conduct two cycles (10 s each) at 6500 rpm with a 5 s pause in between each cycle. Supernatant was collected by microcentrifugation at full speed (13,000 rpm), 4 °C for 2 min and combined in a single PowerSoil® bead tube and vortexed for 15 min. RNA was extracted using proprietary reagents provided in the RNA PowerSoil® Total RNA Isolation Kit per manufacturer instructions (MoBio Laboratories Inc.). RNA samples were treated to remove residual DNA using TURBO™ DNase (Ambion®), Applied Biosystems) following the manufacturer's instructions. Transcriptomic analysis sample RNA concentration was determined using the Agilent 2100 Bioanalyzer system and Agilent RNA Pico 6000 kit (Agilent Technologies Limited, Cheshire, UK).

Dynabeads® kit (Ambion, Life Technologies) and a MagnaBot® II Magnetic Separation Device (Promega) was used to purify mRNA from total RNA samples based on oligo (dT)25 polyA isolation. Purified mRNA integrity and quantity was then assessed using the Agilent 2100 bioanalyzer system and RNA Pico 6000 kit, to ensure samples met the requirements of 0.1 ng mRNA within an 8 μl sample for the SMARTer® cDNA synthesis kit (Clontech Laboratories Inc, US).

2.3.3. mRNA and cDNA preparation

The SMARTer® stranded kit first-strand cDNA synthesis protocol for fragmented RNA samples was followed. Purification of first-strand cDNA from unincorporated nucleotides and small cDNA fragments was carried out using paramagnetic solid phase reversible immobilisation beads (SPRI) from AMPure® (Beckman Coulter Ltd, High Wycombe, UK). Contaminants were then removed by magnetic separation and bead samples were used directly for RNA-seq library amplification. Due to the low input of RNA, each of the purification steps was repeated to ensure complete removal of adapter primers. cDNA samples were eluted in 20 μl nuclease-free water.

Purified first-strand cDNA was amplified into RNA-seq libraries using SeqAmp DNA polymerase (Clontech Laboratories Inc, USA), the universal forward PCR primer and reverse PCR primers from Illumina

indexing primer set. A master mix of 25 μl 2X SeqAmp PCR Buffer, 1 μl Universal Forward PCR Primer (12.5 μM), 1 μl Reverse PCR Primer (12.5 μM), 1 μl SeqAmp DNA Polymerase, and 22 μl nuclease-free water was prepared for each reaction. The reverse PCR primer used was different for each sample so that each had an individually associated indexing sequence. Samples were placed in a preheated (94 °C) Bio-Rad thermal cycler with a heated lid for 1 min and cycled at 98 °C for 15 s, 55 °C for 15 s and 68 °C for 30 s for eighteen cycles. The amplified RNA-seq library was purified by immobilizing onto AMPure® SPRI beads as before with selective binding of first-strand cDNA and removal of contaminants by magnetic separation following manufacturer's instructions. DNA was eluted in 20 μl SMARTer® Stranded Elution Buffer and 1 μl of the amplified RNA-seq library was diluted with 3 μl SMARTer® Stranded Elution Buffer for validation using the Agilent 2100 Bioanalyzer system and a high sensitivity DNA chip. Successful cDNA synthesis and amplification required each sample to show no product yield in the negative control with a distinct peak spanning 150–1000 bp peaking at 300 bp for the positive control (yielding >7.5 nM RNA-seq library, see Supplementary material).

2.3.4. Transcriptome sequencing and analysis

All cDNA libraries were sequenced and analysed by the NERC Biomolecular Analysis Facility (NBAF) at the Centre for Genomic Research, Liverpool University, UK. The template DNA was denatured per the protocol described in the Illumina cBot user guide. The sequencing was carried out on one lane of an Illumina HiSeq2500 at 2x125 bp paired-end sequencing with v4 chemistry. Basecalling and de-multiplexing of indexed reads was performed by CASAVA version 1.8.2 (Illumina) to produce 9 samples from 1 lane of sequence data, in Fastq format. The raw fastq files were trimmed to remove Illumina adapter sequences using Cutadapt version 1.2.1 (Martin, 2011). The option "-O 3" was set, so the 3′ end of any reads which matched the adapter sequence over at least 3 bp was trimmed off. The reads were further trimmed to remove low quality bases, using Sickle version 1.200 with a minimum window quality score of 20. After trimming, reads shorter than 10 bp were removed. All trimmed sequences and processed files can be accessed through the NCBI GEO repository accession GSE245088.

Hypholoma fasciculare was not sequenced at the time of analysis so reference genome fasta files for *Hypholoma sublateritium* (http://genome.jgi.doe.gov/Hypsu1/Hypsu1.home.html) and *Trametes versicolor* (http://genome.jgi.doe.gov/Trave1/Trave1.home.html) (Floudas et al., 2012) were combined and used as a general sequence reference. A gtf file was constructed from the two separate gtf files and resulting file contained 32207 genes. A sequence index was built using HISAT2, and splice site information was extracted and written using functionality provided by HISAT2. R1/R2 read pairs were mapped to the reference sequence using HISAT2 version 2.0.3beta (Kim et al., 2013; Kim et al., 2015). Paired-end mapping was carried out using default parameters except for the option "–score-min L,-0.6,-0.6" which is the same as bowtie2 defaulted – score-min, "-q" for fastq data and "–rf" for first stranded library (Langmead and Saltzberg, 2012). The primary alignment of each mapped read was extracted and classified as an accepted hit, and subsequently utilised for downstream analyses.

Differential transcripts between samples were calculated from reads alignment files using HTSeq count (Anders et al., 2015). The count number was also converted into FPKM values and count numbers per gene were used as input for differential expression analysis. Data variation assessment, data modelling, model fitting, testing and differential gene expression detection were carried out according to established protocols (Glaus et al., 2012; Trapnell et al., 2012). All the differential gene expression analyses were performed in R (version 3.2.2) environment using edgeR (Robinson et al., 2010). As variations of the count data were modelled by a negative binomial distribution, a generalized linear model (GLM) was used (Nelder and Wedderburn, 1972) containing 3 parameters representing the mean expression of corresponding sample groups. The $\log_2$ fold change (FC) values for the required comparisons of sample groups were computed based on the model fitting results and data normalisation factors were calculated to correct for differences in library size among samples. The Trimmed Mean M-values method in edgeR was applied with default parameters and common, trended and tag-wise dispersion parameters were estimated (significance testing). The GLM model was parametrized using the count data and then used to obtain the logFC values for each required comparison. The estimated $\log_2$ FCs were tested in edgeR using a likelihood-ratios test (Wilks, 1938). P-values associated with logFC were adjusted for multiple testing using the false discovery rate approach (Benjamini and Hochberg, 1995). Significantly differentially expressed genes were defined as those with false discovery rate-adjusted P-value < 0.05. Functional characterisation of each differentially regulated transcript was carried out using online database comparisons and annotation information available via the Joint Genome Institute's Mycocosm genome portal.

2.3.5. Protein extraction for peptide analysis

Initial extracellular protein extraction from freeze-dried wood blocks was conducted following adaptation of methods used to extract protein from wood wafers by Dawson-Andoh and Morrell (1992). Sawdust was collected with a sterile grated plane as with RNA extraction and placed in sterile Falcon tubes on ice. Samples were gently agitated in the 30 ml sodium acetate buffer solution (50 mM, pH 5.2) at 4 °C for 12 h. Samples were filtered through sterile glass wool and Whatman® filter paper and the solution collected filtered further through a sterile 0.2 μl filter membrane unit (Millipore Amicon). The extracts were transferred to 3 KDa centrifugal filter units (Millipore Amicon) and centrifuged at × 3.5G at 4 °C for 10 min cycles until concentrated to a 2 ml volume. Concentrated sample solutions were transferred to ultracentrifuge compatible tubes, −20 °C acetone (100%) was added (4x sample volume) and centrifuged (Beckman Coulter; rotor J20, × 9.5G) for 60 min. The supernatant was discarded, and protein pellet re-suspended in 300 μl acidic sodium acetate buffer with added non-ionic detergent (50 mM, pH 5.2, 0.05% v/v TWEEN® 80).

Protein extracts were treated with a protease inhibitor cocktail (Promega) according to the manufacturer's instructions and protein concentrations determined using the Bradford method (Bradford, 1976) using a Biotek Synergy H1 plate reader (595 nm) and calibrated against a bovine serum albumin (BSA; Sigma-Aldrich) standard curve. Sample extracts were concentrated by freeze drying so that the highest possible equal protein concentration of each sample extract could be subsequently analysed.

2.3.6. Preparation of protein extracts for mass spectrometry analysis

Sodium dodecyl sulphate polyacrylamide gel electrophoresis (SDS-PAGE) was used to denature and separate extracted proteins. Laemmli sample buffer (62.5 mM Tris-HCl, pH 6.8, 2% SDS, 25% glycerol, 0.01% Bromophenol blue, 5% 2-Mercaptoethanol) was added to protein extracts so that each sample contained 20 μg of protein in 10 μl of sample buffer, and heated for 10 min at 95 °C. Samples were agitated, allowed to cool and applied to a 12% 1-D SDS-PAGE gel for electrophoresis. Gels were the fixed for 1 h in 50% (v/v) methanol: 10% acetic acid solution and rinsed with ultrapure water (Gibco). Colloidal Coomassie G-250 (34% (v/v) methanol, 2% (v/v) phosphoric acid, 17% (w/v) ammonium sulphate and 0.066% (w/v) Coomassie G-250) was used to stain overnight. Each gel was then de-stained for 90 min in ultrapure water on a shaking platform. Protein band detection was performed using the Bio-Rad Image Lab™ software (v 5.1) package. Protein bands were visualised using automatic band detection with sensitivity of 100% and manually adjusted for individual gels. Protein bands were excised into individual nuclease-free non-stick tubes and washed in 100% acetonitrile (ACN). Excised protein samples were dried using a SpeedVac centrifuge (Eppendorf) for 30 min and in-gel digested overnight at 37 °C with Trypsin Gold (20 μg ml^{-1} in 40 mM NH_4HCO_3/10% ACN), following manufacturer's guidelines (Promega).

2.3.7. MALDI-ToF analysis

Digested protein samples were collected to dryness in a SpeedVac centrifuge (Eppendorf), resuspended in 10 μl 0.1% formic acid. A matrix solution was then prepared with 10 mg ml^{-1} cyano-4-hydroxycinnamic acid (CHCA) in 50% ACN and 0.1% Trifluoric acid (TFA). 1 μl of matrix solution and 1 μl of each sample was spotted onto a Perseptive Biosystems 96-well MALDI plate. A calibration solution was also prepared in which 0.33 mg ml^{-1} of known peptides (des-Arg-Bradykinin, Angiotensin 1 and Glu-finrinopeptide B) were combined to produce a 1 mg ml^{-1} mixture. Calibration mixture (2 μl) was combined with 100 μl matrix solution and 1 μl spotted onto MALDI plates. Prepared plates were air dried for analysis. MALDI-ToF analysis was carried out using a Voyager DE-STR instrument (Applied Biosystems, UK) in reflectron mode with an acceleration voltage of 20,000 V, grid voltage of 95% of the acceleration voltage, a delay time of 200 nsec and 100 laser shots per spectrum. MS spectra were acquired over a mass range of m/z 800–4000 and final mass spectra were internally calibrated using the tryptic autoproteolysis products at m/z 842 and 2122 using Data Explorer.

2.3.8. Liquid chromatography-mass spectrometry (LC-MS) analysis

Digested protein samples were dried in a SpeedVac centrifuge (Eppendorf), resuspended in 25 μl 0.1% formic acid and transferred to vials for LC-MS analysis. Standard samples were included in LC-MS analyses to ensure that all columns were clear and LC-MS sensitivity accurate. For LC-MS analysis, 5 μl protein sample was injected onto a pepmap HPLC column (Thermoscientific, UK) with dimensions 25 cm length, 300 μm internal diameter via a mobile phase flow rate of 4 μl min^{-1} utilising an Ultimate 3000 HPLC system (Thermoscientific, UK). The mobile phases were A, 98%/2% water with 0.1% formic acid/acetonitrile with 0.1% formic acid and B, 100% acetonitrile with 0.1% formic acid. The gradient applied during separation was 0–5 min in 100% solution A, with subsequent gradient changes of 5–20 min in 20% solution B, 20–45 min in solution B, 45–55 min in 100% solution B, 55–60 min in 100% solution A, and 60–90 min in a re-equilibration of the column in 100% A. Eluent from the HPLC column was analysed using a DECA-XP LCQ Ion Trap mass spectrometer (Thermoscientific, UK) with a spray voltage of 3.5 kV, a capillary voltage of 10V and a capillary temperature of 185 °C. The mass spectrometer was operated in data dependent mode, undertaking a full scan between 475 and 2000 Da, followed by MS/MS of the three most abundant peaks using a collision gas of 32% arbitrary units and a dynamic exclusion list of 25 peaks within a 3-min period. Mass spectrometry data was deposited on the Open Science Framework repository (https://osf.io/ywf8h/?view_only=2066e12645c44fd4bf3508f5b8a6e8e0).

2.3.9. Identification of proteins based on MALDI-TOF and LC-MS analysis

Mass spectral data obtained from both MALDI-TOF and LC-MS were submitted to database searching using a locally running copy of the Mascot program (Matrix Science Ltd., version 2) to identify the maximum number of matched peptides. Spectral data were submitted to peptide mass fingerprint search through the Applied Biosystems GPS Explorer software interface to Mascot. Search criteria included: Maximum missed cleavages, 1; no fixed modification, variable modifications: Oxidation (M); Peptide tolerance, 10 pmm. Matched peptides were aligned to and searched against *Trametes versicolor* specific sequences using the NCBI protein BLAST programme (http://blast.ncbi.nlm.nih.gov/Blast.cgi). For identification by MALDI peptide mass fingerprinting, multiple peptides derived from the same protein were required to fall within the 10 ppm mass tolerance window. For LC-MS, identification was based upon at least one peptide match, matching intact peptide m/z and sufficient b and y ion coverage of the fragment ions formed and a P value of <0.05 in the MASCOT search output.

3. Results

3.1. Growth characteristics and wood decay rate in microcosms

In all microcosms, *Hypholoma fasciculare* emerged from its originally colonised wood blocks within 5 days. Mean extension rate over the soil surface for 25 days (2.834 cm d^{-1}) was not significantly different between single species pairings and in microcosms with *T. versicolor* colonised blocks. The mean decay rate ($mg.cm^3.d^{-1}$) was greater for wood blocks where *T. versicolor – H. fasciculare* interactions took place (5.21 ± 0.168) than for single species paired microcosm blocks (Tv single species $= 3.90 \pm 0.106$; Hf single species $= 2.50 \pm 0.130$) and the *H. fasciculare* inoculum wood block in the interaction microcosms ($=2.8220 \pm 0.1210$) (Supplementary Tables S2 and S3).

3.2. Transcriptome analyses

A low quantity of RNA was extracted from all samples, i.e. below 0.067 μg μl^{-1} required for direct Illumina HiSeq 2500 sequencing, however, they all generated cDNA libraries of sufficient quality for sequencing following mRNA purification and cDNA library amplification (Supplementary Figs. S1 and S2). Forward and reverse read paired libraries were mapped to the relevant reference genomes following initial quality assessment and processing using the CGR pipeline (Supplementary Figs. S3–S7 and Tables S4–S6). The number of trimmed read pairs varied between 44,348,974 and 69,333,160 reads and the percentage of reads mapped to the reference genomes varied between 29.4 and 71.8%. Reads obtained from the *T. versicolor – H. fasciculare* interaction blocks showed lower alignment percentages (29.4–50.2%) than the single species paired microcosm samples (all over 60% alignment). Analysis of count data variation between samples (comparing log10 gene expression) showed a correlation between replicates of <0.7, and gene feature mapping analysis showed that the majority of reads aligned gene features as expected (Supplementary Figs. S4–S7, Table S5).

A negative binomial distribution model of count numbers provided a differential expression analysis using a generalized linear model where the mean expression of the three treatment groups as parameters was used to obtain the logFC values for comparison. Fold change (log_2FC) were compared against the expression level counts per million mapped reads (Supplementary Figs. S6-S7, Table S6). There were significantly differentially expressed transcripts (FDR-adjusted P-value $<5\%$) in the interaction wood blocks compared with those from single species pairings. Up- and down-regulated transcripts with a 3-fold or greater change were selected for functional assessment. From 226 transcripts identified, 104 mapped to the *T. versicolor* genome and 122 to the *H. sublateritium* genome, of which 70/34 and 94/29 transcripts were either up/down-regulated in *T. versicolor* and *H. fasciculare* respectively when compared with single species pairings. Fold-change expression values ranged from 7.13 to −5.65 for *T. versicolor* (Table 1) and 22.6 to −6.63 for *H. fasciculare* (Table 2).

3.3. Functional characterisation of differentially regulated transcripts

Twenty-five percent of the *T. versicolor* and 24.6% of the *H. fasciculare* differentially expressed transcripts were without hypothetical proteins without functional annotation (Table S6). Three *T. versicolor* and eight *H. fasciculare* transcripts appeared to be lineage specific based on no positive BLAST hit against other species. Interestingly, the three most upregulated interaction-associated transcripts for *T. versicolor* were without functional annotation. The remaining differentially regulated transcripts were characterised using eukaryotic orthologous groups (KOGs) descriptors to define biological function during interactions, particularly where multiple functions may be present for some transcripts (Fig. 2).

For *T. versicolor*, more transcripts were annotated as *cellular processes*

Table 1
T. versicolor differentially regulated transcripts during the interaction with *H. fasciculare* compared to self-interaction paired blocks. Protein id numbers relate to the *T. versicolor* v1.0 genome annotation from the JGI Mycocosm portal. Downregulated transcripts are highlighted in grey.

Protein id	Putative gene function	Fold change
	Information, storage & processing	
Translation, ribosomal structure & biogenesis		
60526	KRR1-interacting protein involved in 40S ribosome biogenesis	6.25
110730	EF-1 translation elongation factor	5.21
37646	4F translation initiation factor	-4.66
RNA processing & modification		
44224	EVE domain protein associated with RNA binding (IPR002740)	5.67
35448	Wtap pre-mRNA splicing regulator	4.36
158285	SF3A2 splicing factor protein with conserved C2H2 Zn finger domain	-4.83
54839	Subunit of SF3A splicing factor complex with C2H2 Zn finger domain	-4.70
65239	WD40 repeat protein of the nuclear pore Nup82 subcomplex	-4.43
Transcription		
29680	Putative fungal transcriptional regulatory zinc finger protein	5.36
171344	Basic helix-loop-helix (bHLH) protein, similarity to myc-family transcription factors	5.32
63636	LIM domain protein calcium-responsive transcription co-activator	-5.15
38742	Aminoacyl-tRNA synthetase, class I	-4.50
Replication, recombination & repair		
165502	DNA polymerase III (delta) subunit	5.67
47761	SNF2 family DNA-dependent ATPase helicase enzyme	3.04
Chromatin structure & dynamics		
166025	Histone deacetylase and subunit of Set3 and Rpd3L complexes	5.63
74747	SUMO-like domain 2 protein	4.95
164879	DNA (cytosine-5-)-methyltransferase	-4.78
	Cellular Processes & signalling	
Cell cycle division		
67715	Filamentation induced by cAMP protein Fic	5.83
Cell wall / membrane /envelope biogenesis		
37684	Subunit of the glycosylphosphatidylinositol transamidase complex	5.70
57434	Mitochondrial ADP/ATP carrier protein	5.63
142601	DUF124 protein linked to biogenesis and organisation of mitochondrial membranes	5.51
Cytoskeleton		
122881	Kinesin-like motor protein	-4.67
Intracellular trafficking, secretion & vesicular transport		
109941	Armadillo-fold motif similar to protein and nucleic acid-binding symportin	5.87
159612	Subunit C V1 peripheral endomembrane vacuolar H+-ATPase	5.81
27977	GTP-binding protein involved in nuclear protein transport	5.25
25487	SNARE protein SED5/Syntaxin 5	-4.79
21099	SNARE-associated integral membrane protein of the Golgi complex	-4.72
63914	Autophagy-related diacylglycerol pyrophosphate phosphatase	-4.29
Posttranslational modification, protein turnover & chaperones		
49395	Thioredoxin	6.42
121349	Glutathione S-transferase	6.13
71097	Cyclin-F F-box domain protein associated with intracellular protein degradation	5.90
71710	AAA ATPase subunit of the polyubiquitin-selective segregase complex	5.49

and signalling (33.7%), with 25.0% annotated under *metabolism*, and 16.3% under *information storage and processing* (Fig. 2A). For *H. fasciculare*, *cellular processes and signalling* was similarly highly represented at 30.3%, while transcripts annotated under *metabolism* were lower at 19.7% than *information storage and processing* at 26.2% (Fig. 2A).

3.3.1. Cell processing and signalling KOG category profile

Transcripts annotated under the *posttranslational modification, protein turnover and chaperones* category were prominent for both fungi during their interaction, with 13 out of 34 for *T. versicolor* and 16/37 for *H. fasciculare* (Fig. 2B). *Signal transduction* mechanisms were also differentially regulated strongly for *T. versicolor* (ten gene annotations). Surprisingly a single transcript was annotated under defence mechanisms for either fungus, a putative alkyl-hydroperoxide reductase gene (IPR000866) upregulated in *H. fasciculare*, although a thioredoxin (IPR005746) with putative antioxidant protection activity was highly upregulated in *T. versicolor*.

Protein turnover was evident in the *T. versicolor* interaction response (Table 1) with two proteinases (IPR008758/021109) and three cyclin-like F-box proteins (IPR001810) linked to E3 ligase function upregulated, however, an E3 ligase gene (IPR010309) was also downregulated. Alteration in signal transduction was also recorded with five protein kinases (four serine/threonine protein kinases; IPR000719/009056/011009/040976) and AAA ATPase associated with the polyubiquitin-selective segregase complex involved in the assembly of signalling complexes (IPR005938/yeast ortholog S000002284) upregulated. While other signalling transcripts were down regulated, including a

27286	COX15-like protein associated with cytochrome c assembly	5.42
71894	Cyclin-F F-box domain protein associated with intracellular protein degradation	5.04
21852	Conserved Cyclin-like F-box domain protein	4.74
166319	Serine carboxypeptidase S28	4.74
67128	F-box motif protein with SkpI domain, associated with ubiquitin E3 ligase function	4.73
21449	Aspartic peptidase	4.64
32015	Glycosyltransferase family 69 protein α-1,3-mannosyltransferase	-4.52
27987	AAA ATPase protein translocase and chaperone required for Complex III assembly	-4.45
69070	HECT-type E3 ubiquitin-protein ligase	-4.05
129640	S53 Sedolisin serine carboxypeptidase	-4.85
Signal transduction		
131991	Fungal-type protein kinase	5.58
23945	Serine/threonine protein kinase	5.44
44951	Serine threonine protein kinase	5.14
61484	GTPase-activating protein (GAP), putative subunit of SEA and Iml1p complexes	3.26
45166	Serine/threonine protein kinase	-3.43
30303	Serine/threonine protein kinase	-2.84
Metabolism		
Amino acid transport & metabolism		
47221	Serpin-like protease inhibitor I4	5.77
46171	Phenylpyruvate tautomerase	5.77
126310	Major facilitator superfamily MFS-1 Polyamine transporter	5.77
171167	Methionine/cysteine permease	5.50
30009	Gamma-aminobutyrate (GABA) permease	3.97
53504	Major facilitator superfamily MFS-1 Allantoate/dipeptide permease	-4.95
Carbohydrate transport & metabolism		
159764	Dienelactone hydrolase	-4.79
25899	LysM domain protein with peptidoglycanase and chitinase-associated activity	-4.51
73840	Galactose oxidase central KELCH 4 domain-containing protein	-4.55
Energy production & conversion		
134768	YVTN repeat-like quinoprotein amine dehydrogenase	6.35
37734	Alcohol dehydrogenase	5.87
151087	Alcohol dehydrogenase	5.67
144542	Subunit d of the stator stalk of mitochondrial F1F0 ATP synthase	5.19
61500	β-subunit of the F1 sector of mitochondrial F1F0 ATP synthase	5.05
158886	Succinyl-CoA synthetase β-subunit	-5.37
Inorganic ion transport & metabolism		
137982	Molybdenum cofactor sulphurase, MOSC motif sulphur carrier	5.87
73562	Hemerthryin family-like protein associated with oxygen transport	5.67
121157	ER-localised heme oxygenase (heme turnover during iron limitation)	5.29
27121	Acid phosphatase	-5.65
Lipid transport & metabolism		
114756	Carboxyesterase, Acetylcholinesterase/Butyrylcholinesterase activity	6.29
130844	Cytochrome P450 E1	5.87
173014	Cytochrome P450 E1	5.47
150386	Steroid reductase, structural prediction: 3-oxo-5,α-steroid-4-dehydrogenase	5.09
167853	Hormone-sensitive lipase	-4.98
174308	Carboxyesterase type B lipase	-4.62
Secondary metabolites biosynthesis, transport & catabolism		
47002	Isoprenoid synthase domain protein of class I terpene cyclases	6.42

putative serine/threonine protein kinase (IPR002290) and stress response-associated MAP kinase (IPR000719).

Seven transcripts upregulated in *H. fasciculare* interaction wood blocks (Table 2) were associated with protein breakdown and turnover; three proteinases (IPR009007/011600/015366), two ubiquitin-conjugating enzymes (IPR00608), an N-end rule pathway protein (IPR039733) and Zinc finger protein (IPR001841) both associated with ubiquitin-dependent proteolysis. While three other downregulated genes had putative function associated with protein N-glycosylation and protein maturation or progression through the endoplasmic reticulum and Golgi apparatus (Swp1 N-oligosaccharyl transferase complex protein IPR008814, Glycosyl hydrolase family 92 α-1,2-mannosidase IPR012939 and cytoplasmic thioredoxin IPR006662).

3.3.2. *Information storage and processing KOG category profile*

The *H. fasciculare* interaction response was more prominent under this class with *translation, ribosome structure and biogenesis* and *RNA processing and modification* represented strongly (Fig. 2B). Four transcripts putatively associated with the formation, transport or structure of the 90S pre-ribosome or 60S ribosome (IPR003593/007718/027145/027417/028599) were upregulated, along with a ribosomal lysine methyltransferase (IPR001214) and mitochondrial ribosomal L5P family protein (IPR002132, Table 2), indicating a response involving protein biosynthesis. In addition, a relatively high number of transcripts (five) putatively associated with RNA lysis/turnover were upregulated, namely 2 RNAase H enzymes (IPR002156), a component of the cleavage of polyadenylation factor I (IPR000504), a mRNA decapping hydrolase (IPR008594) and a Pumilio repeat RNA binding protein (IPR001313) associated with mitochondrial mRNA degradation. While four enzymes

Table 2
H. fasciculare differentially regulated transcripts during the interaction with *T. versicolor* compared to self-interaction paired blocks. Protein id numbers relate to the *H. sublateritium* genome annotation from the JGI Mycocosm portal. Downregulated transcripts are highlighted in grey.

Protein id	Putative gene function	Fold change
	Information, storage & processing	
Translation, ribosomal structure & biogenesis		
90682	RNA synthetase class II, aminoacyl-tRNA synthetase	5.73
192621	Ribosomal L5P family C-terminus, mitochondrial ribosomal protein	5.57
42872	Impact family motif protein translation regulator	5.53
61592	Ribosomal methyltransferase	5.26
65038	AAA ATPase pre-ribosomal nuclear export complex associated	5.06
52097	SRP40/nopp40-like protein involved in pre-ribosome assembly / transport	4.74
140767	WDR12/Ytm1 protein, component of the NOP7 complex 25/5.8S rRNA maturation	4.52
201695	Periodic tryptophan protein, conserved 90S pre-ribosomal component	4.23
38707	Ribosomal protein L3	-3.98
RNA processing & modification		
182835	mRNA cleavage and polyadenylation factor I complex, subunit RNA15	22.6
1069895	RNAse H ribonuclease	7.00
993395	Pumilio RNA-binding domain translational repressor protein	6.71
50272	FOG RNA recognition motif (RRM) protein of unknown function	5.83
46852	Scavenger mRNA decapping enzyme DcpS/DCS2	5.71
127265	RNA polyadenylation polymerase	5.42
32927	RBM-like pre-mRNA Splicing factor	4.90
180488	RNAse H ribonuclease	2.99
34873	FOG RNA recognition motif (RRM) protein of unknown function	-6.63
34557	Pre-mRNA processing factor Prp40	-4.13
68660	DEAD/DEAH box helicase	-4.11
40013	Sen15 motif conserved protein with tRNA intron-splicing endonuclease activity	-3.31
Transcription		
38139	C2H2 Zinc finger protein	7.34
43588	Fungus-specific transcription factor domain protein	6.16
150144	FOG C2H2 Zinc finger protein	5.71
83651	Fungus-specific Zn(2)-C6 DNA-binding domain protein	5.20
Replication, recombination & repair		
615380	P-loop containing nucleoside triphosphate hydrolase	6.25
144961	Integrase-like DNA breaking-rejoining enzyme	5.42
62394	DNA polymerase α-subunit	4.21
1084208	Transposase with En/Sp-like motif	4.87
Chromatin structure & dynamics		
67307	TET family deoxygenase (DNA 5-methylcytosine oxidation)	5.95
38036	BTB/POZ domain transcriptional regulator	5.25
146037	SET domain histone methyltransferase COMPASS subunit	5.06
	Cellular Processes & signalling	
Cell cycle division		
38340	WD40 repeat Cdc20 family protein anaphase-promoting, cell cycle activator	5.25
144552	Sister chromatid cohesion protein Pds5	5.21
1014314	LYAR-type C2H2 Zinc finger cell growth-regulating nucleolar protein	5.21
Cell wall/ membrane /envelope biogenesis		
133093	Glycoside hydrolase family 17 probable glucan 1,3-β-glucosidase	5.08
127578	Glycoside hydrolase family 72 β-1,3-glucanosyltransferase	4.90
144365	Glycosyltransferase 2-like domain protein	-4.01
Cytoskeleton		
81360	γ-tubulin complex component protein	5.69
196179	α-tubulin	3.40
138804	Actin-related protein Arp2/3 complex subunit ARPC5	-4.58
Defense mechanisms		
38377	Peroxiredoxin-like alkyl hydroperoxide reductase	5.84
Intracellular trafficking, secretion & vesicular transport		
38618	AAA-ATPase VPS4-associated endosomal protein 1	5.95
165994	Vacuolar H^+-ATPase of the V0 complex	5.94
145151	WRB/Get1 family motif protein associated with ER/Golgi function	5.66
211221	UV radiation resistance protein/autophagy-related protein Atg14	5.11
36252	Vacuolar sorting protein 36 (Vps36) subunit of ESCRT-II	-4.19
126350	Dynein light chain Tctex-1-like protein	-4.08

Posttranslational modification, protein turnover & chaperones		
45486	FOG:FHA domain Zinc finger C3HC4 protein associated with ubiqutination	6.78
631643	F-box WD40/YVTN repeat-like domain superfamily	6.58
192041	ubiquitin-protein ligase	6.06
126190	RWD-like ubiquitin-conjugating enzyme E2	5.95
79148	Protein N-terminal glutamine amidohydrolase of the N-end rule pathway	5.84
62513	DnaJ-like chaperone	5.71
61236	Caspase-like domain superfamily protein (cysteine peptidase)	5.18
216857	Molecular chaperone of the HSP70 superfamily	4.96
37633	UDP-glucose:glycoprotein glucosyltransferase (Glycosyltransferase family 24)	4.51
72858	Aspartic peptidase	3.68
126856	S53 Sedolisin serine carboxypeptidase	3.45
45274	Swp1 subunit of the N-oligosaccharyl transferase (OST) complex	-4.98
67848	Glycoside hydrolase family 92 α-1,2-mannosidase	-4.25
35566	Thioredoxin	-4.22
643624	F-box domain protein	-4.03
617407	F-box domain protein with RNI-like motif	-3.53
Signal transduction		
51910	Serine/threonine-protein kinase	5.06
71457	ADP-ribosylation factor (Arf) GTPase activating protein	4.91
139092	Organic solute transporter subunit alpha/Transmembrane protein 184	3.81
67110	PLC-like phosphodiesterase superfamily domain protein	-4.06
836395	Protein kinase	-3.49
Metabolism		
Amino acid transport & metabolism		
42398	Dihydroxy-acid dehydratase	-4.00
Carbohydrate transport & metabolism		
67123	Galactose permease sugar transporter	6.34
126797	Glycoside hydrolase family 18 Chitinase	5.84
38206	Glycoside hydrolase family 79 Glucuronidase activity	5.71
39467	Glycoside hydrolase family 5 subfamily 12 Glucanase / cellulase activity	5.35
196947	Glycoside hydrolase family 28 endo-polygalacturonase	5.25
32409	Glucose-6-phosphate dehydrogenase	4.89
169432	Bicupin domain, oxalate decarboxylase/oxidase protein	-4.74
Coenzyme transport & metabolism		
623648	General superfamily transporter and Pantothenate transporter FEN2	5.06
188285	Haloacid dehalogenase(HAD)-like superfamily / pyridoxal phosphate phosphatase	-4.15
61139	Dihydrofolate reductase	-4.09
41936	S-adenosyl-L-homocysteine hydrolase	-4.07
Energy production & conversion		
37110	Pyruvate carboxylase	-3.97
32578	NADH:Ubiquitone reductase, NDUFA5/B13 subunit	-3.76
Inorganic ion transport & metabolism		
378629	Histidine phosphatase superfamily clade-2 domain protein / acid phosphatase	5.17
1065361	Vacuolar Ca^{2+} ATPase	4.41
Lipid transport & metabolism		
31547	Cytochrome P450 E-class iV	4.76
74601	Carboxylesterase	4.40
Secondary metabolites biosynthesis, transport & catabolism		
217612	Cytochrome P450 E class I	5.25
55504	Short-chain dehydrogenase/reductase SDR	5.25
188119	FAD-binding domain protein with conserved Berberine/berberine-like domain	5.22
40211	Short-chain dehydrogenase/reductase SDR	4.91
63026	Non-ribosomal peptide synthetase/α-aminoadipate reductase	4.55
45142	Nitronate monooxygenase	-4.17

putatively associated with RNA processing and transport were downregulated, a pre-mRNA spliceosome processing protein (IPR002713), tRNA intron-splicing endonuclease (IPR018593), a DEAD box helicase (IPR011545) and a possible polyadenylation binding/stabilisation protein (IPR000504, Table 2).

Evidence of a coordinated strategy associated with transcription and translation was not apparent for *T. versicolor*; each category had two upregulated gene annotations and *RNA processing and modification* was the only category that had a greater number of downregulated putative gene transcripts (Fig. 2A). Two putative transcription factors (IPR001138/011598) were upregulated and a cytochrome *b*5-domain calcium-responsive transcription co-activator (IPR001199) was downregulated which may indicate active gene regulatory processes during the interaction with *H. fasciculare* (Table 1).

3.3.3. Metabolism KOG category profile

There was a notable difference in transcription relating to the *metabolism* categories with *T. versicolor* demonstrating a greater metabolic response than *H. fasciculare* (Fig. 2, Tables 1 and 2). *Amino acid transport and metabolism* and *energy production and conversion* were

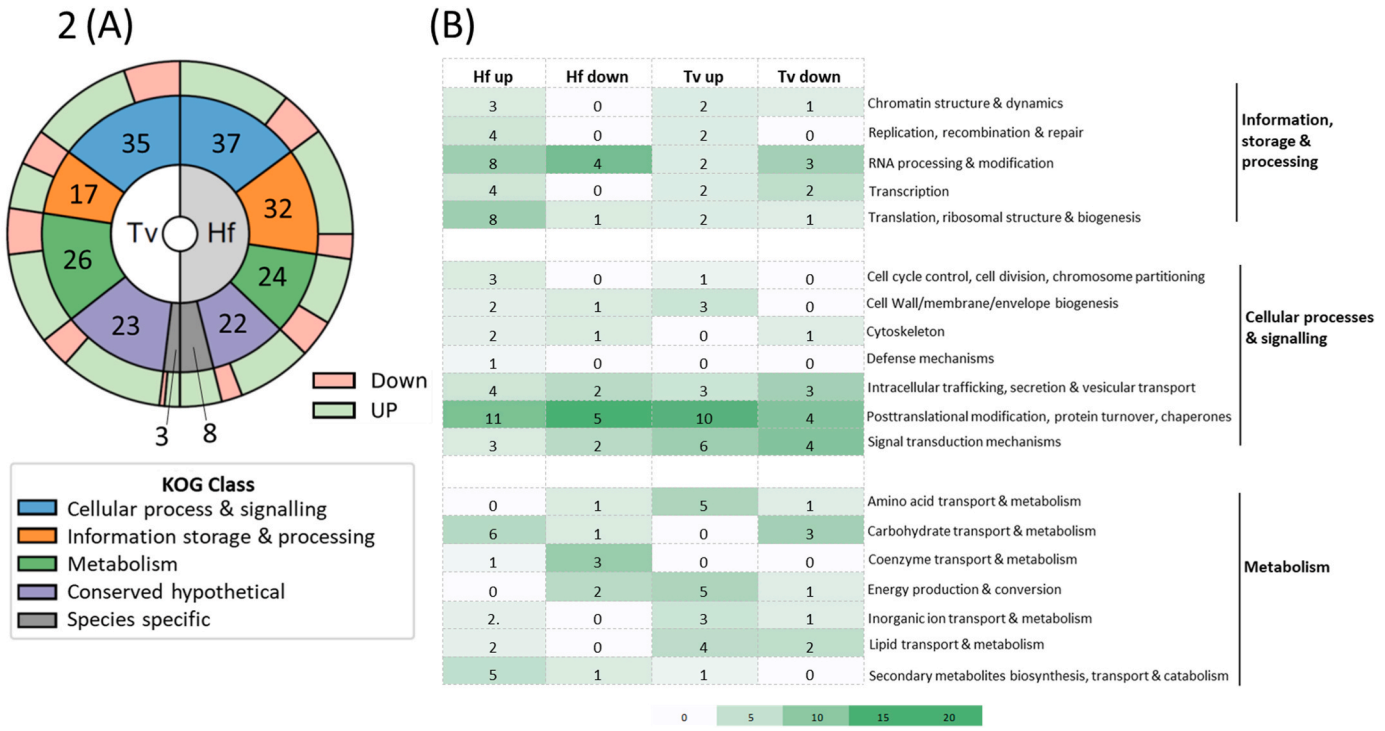

Fig. 2. Functional characterisation of differentially regulated transcripts in *T. versicolor* (Tv)-*H. fasciculare* (Hf) competitive interaction wood blocks. A. Comparison of the proportion of differentially up- and down-regulated transcripts within each KOG functional class for each fungus. Values indicate the number of differentially transcripts in each class. B. Heat map of the relative proportion transcripts of each KOG category represented as a percentage of up- or down-regulated transcripts for each fungus. Samples were collected in triplicate. The absolute number of transcripts within each category is presented.

prominent for *T. versicolor*, while no upregulated gene annotations were made for either of these classes for *H. fasciculare*. In contrast, *carbohydrate transport and metabolism* and *secondary metabolite biosynthesis, transport and catabolism* featured prominently for *H. fasciculare*. The upregulation of transcripts associated with lipid transport and inorganic ion transport and metabolism were recorded for both fungi.

Three of the five upregulated *T. versicolor* interaction gene transcripts putatively annotated under *amino acid transport and metabolism* were permeases/transporters (a general amino acid GABA permease IPR004841, methionine/cysteine permease IPR002293/yeast ortholog S000003287, and a polyamine transporter IPR011701/cd17323) while an allantoate permease (major facilitator superfamily IPR011701) was downregulated. Interestingly, a putative serine proteinase inhibitor (IPR000215) was also upregulated. Two subunits of the F1F0 ATP synthase complex (IPR000194) and two alcohol dehydrogenase (IPR013149) genes were upregulated, while a β-subunit of succinyl-CoA (IPR005809) was downregulated, suggesting a response in energy production and conversion processes in *T. versicolor* when interacting with *H. fasciculare*.

H. fasciculare increased transcription of putative carbohydrate substrate-targeting enzymes, namely three glycosyl hydrolase family enzymes (GH5 subfamily 12 cellulase IPR001547, GH28 pectin-targeting endo-polygalactouronase IPR000743, GH79 arabinogalactan active β-glucuronidase IPR005199) and a putative galactose permease sugar transporter (IPR003663), while an oxalate decarboxylase/oxidase gene (IPR017774) was downregulated. In addition, a GH18 chitinase (IPR001223) associated with both chitin depolymerisation or cell wall remodelling during active growth was also upregulated. In contrast, the three gene transcripts identified in *carbohydrate metabolism* category for *T. versicolor* were all downregulated. *H. fasciculare* upregulated secondary metabolism-associated transcripts included a nonribosomal peptide/α-aminoadipate reductase (IPR009081) implicated secondary metabolite production from lysine in fungi and a flavoenzyme with conserved berberine bridge domain (IPR006094/012951) associated with the biosynthesis of isoquinone alkaloids. A single, highly upregulated terpenoid synthase gene (IPR008949) was identified for *T. versicolor* under this category, which was also the most upregulated functionally characterised *T. versicolor* gene (6.42-fold increase).

3.4. Protein analysis

Sixty-two peptides isolated from interaction and single species control blocks were putatively identified. The majority of proteins identified, 37 of the 62, were present in all treatments (Fig. 3, Table 3, Supplementary Fig. S8). Twelve proteins were identified in the *T. versicolor-H. fasciculare* interaction blocks only (Fig. 3). The remaining 12 proteins were isolated from self-paired control wood blocks, with three proteins common to both fungi, one further protein (a cytochrome P450 enzyme) was identified in both the interaction and *T. versicolor* single species blocks (Fig. 3C). The majority of proteins common to all treatment and competitive interaction-specific wood blocks had metabolic function (64.9% and 58.3% respectively). Triplicate SDS PAGE analysis were undertaken to compare protein profiles based upon gel staining and fractionation of the proteins prior to mass spectrometric analysis in order to reduce the complexity of the protein samples analysed in order to improve protein identification rates. As such, no comparison of protein identification between replicates was undertaken.

3.4.1. Peptides unique to the interaction wood blocks

Energy generation and carbohydrate metabolism associated proteins were identified, including an ATP synthase F1 alpha subunit (IPR000194) also upregulated in the *T. versicolor* interaction transcriptome and a mitochondrial carrier protein (IPR002067) also associated with mitochondrial functioning. Three separate acetyl-CoA synthetase-like proteins (IPR011904) and a lignin peroxidase (IPR024589) isolated from the interaction wood blocks had similar annotation to differently sized peptides described in all treatments (Fig. 3C–Table 3). In addition to a general ABC transporter protein of

unknown function (IPR003439), proteins involved in intracellular vesicular protein transport (clathrin adaptor mu subunit coat protein IPR001392) and posttranslational protein folding (GroES-domain chaperonin 10-like protein IPR020818) were identified. A putative nonsense-mediated mRNA ribonuclease PIN-domain-like protein (IPR029060) and 40S ribosomal subunit maturation-associated DUF663-domain protein (IPR007034/SM01362) were also described.

3.4.2. *Peptides described in all treatment wood blocks*

The peptides common to all the treatment blocks tested, irrespective of interaction status, were dominated by metabolic enzymes largely associated with substrate decomposition and metabolism of released carbohydrates, specifically glycolysis (Table 3). Two enzymes commonly associated with white rot decay (lignin peroxidase and pyranose-2-oxidase IPR012814) were identified along with four glycoside hydrolases (GH28 pectin lyase endo-galacturonidase IPR000743, a hemicellulase GH27 family protein IPR002241, and two GH3 family β-glucosidases IPR036962). Interestingly, the presence of an acetyl-CoA synthetase, acetate-CoA ligase (IPR011904) and a hydroxymethylglutaryl-CoA synthase (IPR010122) may indicate a general activation of the mevalonate-dependent isoprenoid biosynthesis pathway during wood decay by both fungi. Other cellular processes represented in all colonised wood blocks included intracellular trafficking, posttranslational modification, signal transduction and DNA repair proteins.

4. Discussion

This study describes the early transcript and protein expression responses of two competing saprotrophic wood decay fungi under controlled, yet ecologically relevant, microcosm conditions. The physical separation of the wood resources meant that the non-resource limited, late secondary decay species, *H. fasciculare*, had developed an extended corded network before encountering the wood block colonised by *T. versicolor*. This is the first study to assess the effect of spatial separation on the molecular responses to antagonism in wood decay fungi.

4.1. *Wood block experimental design and colonisation measurements*

Wood blocks provide a three-dimensional solid interaction space that cannot be replicated in agar, wood chips or sawdust where colonisation and interactions occur largely on the surface of the substrate. While providing a more representative landscape to assess intraspecific fungal interactions, the setup made it difficult to obtain RNA and insoluble or substrate/membrane bound proteins may also not have been detected (Moody et al., 2018). Limitations accepted, the data presented is robust and give critical insights to intact wood community interactions. Analyses were performed after 14 days following initial *H. fasciculare* contact based on previous work (Hiscox et al., 2018) where both species were likely to be present and actively competing.

The decay rate of *H. fasciculare* blocks in the soil microcosms was significantly greater in wood blocks where *H. fasciculare* competed and

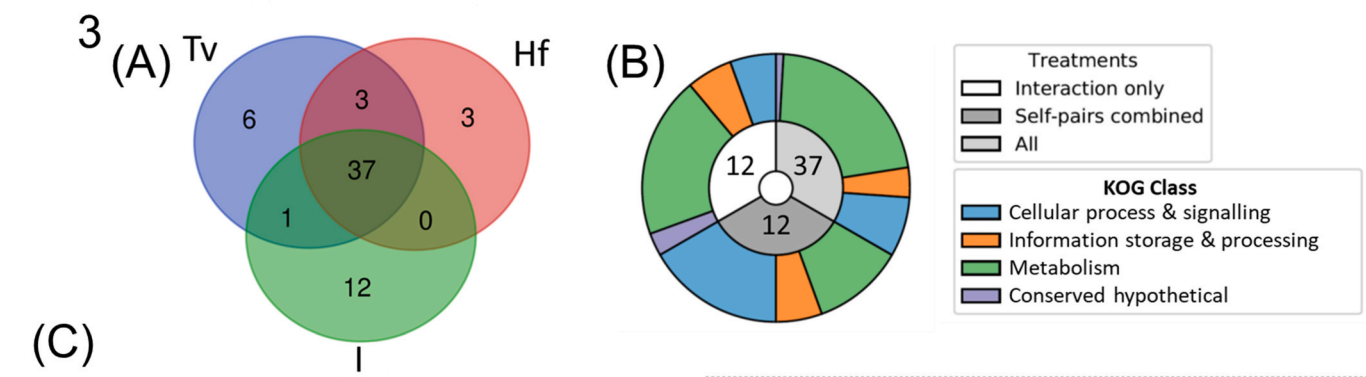

Proteins extracted from interaction blocks only		
Putative function	**KOG Class**	**KOG Category**
ABC Transporter	G	General functional prediction
Mitochondrial carrier protein	M	Energy production & conservation
ATP synthase F1 alpha subunit	M	Energy production & conservation
Para-aminobenzoic acid synthe-	M	Co-enzyme transport & metabolism
3x Acetyl-CoA synthetase	M	Co-enzyme transport & metabolism
Lignin peroxidase	M	Carbohydrate transport and metabolism
DUF663-domain-containing pro-	I	Translation, ribosomal structure & biogenesis
PIN domain-like protein	I	RNA processing and modification
GroES-like chaperone protein	C	Posttranslational modification, protein turnover, chaperones
Clathrin adaptor mu subunit	C	Intracellular trafficking, secretion & vesicular transport
Proteins extracted from *T. versicolor* & *H. fasciculare* self-paired blocks		
Dihydropteroate synthase	M	Co-enzyme transport & metabolism
Cysteine proteinase	C	Posttranslational modification, protein turnover, chaperones
Thioredoxin-domain protein	C	Posttranslational modification, protein turnover, chaperones

Proteins extracted from *T. versicolor self-paired blocks only*		
Putative function	**KOG Class**	**KOG Category**
FMN-dependent alpha-hydroxy acid dehydrogenase	M	Energy production & conservation
O-Acetylhomoserine amine	M	Amino acid transport and metabolism
tRNA isopentenyltransferase	I	Translation, ribosomal structure & biogenesis
DNA-dependent RNA polymerase (β & β′ subunits)	I	Transcription
Protein disulfide isomerase	C	Posttranslational modification, protein turnover, chaperones
Clathrin adaptor mu subunit	C	Intracellular trafficking, secretion, and vesicular transport
Proteins extracted from *H. fasciculare self-paired blocks only*		
2-Isopropylmalate synthase	M	Amino acid transport and metabolism
SRP-like signal recognition protein	C	Intracellular trafficking, secretion & vesicular transport
Vesicle budding-like protein	C	Intracellular trafficking, secretion & vesicular transport
Proteins extracted from Interaction & *T. versicolor self-paired blocks*		
Cytochrome P450	M	Lipid transport and metabolism

Fig. 3. Functional characterisation of peptides extracted from *T. versicolor* (Tv)-*H. fasciculare* (Hf) interaction wood blocks. A. Distribution of common and treatment-specific peptides. I indicates interaction-specific peptides contrasted with self-pared (Tv/Hf) controls. B. Comparison of the proportion of peptides within each KOG functional class present in different interaction treatment groups. C. Functional description of peptides isolated in specific interaction samples with relevant KOG class and category descriptors. Triplicated samples were analysedKOG class key C: Cellular processing and signalling; G: General function prediction; I: Information storage and processing; M: metabolism.

Table 3
Functional characterisation of proteins extracted from all interaction blocks.

Putative function	KOG Category
General Function	
GTP-binding protein	General Function
Metabolism	
2x O-Acetylhomoserine amine	Amino acid transport & metabolism
Phosphoserine aminotransferase	Amino acid transport & metabolism
Aldolase	Carbohydrate transport & metabolism
B-glucosidase	Carbohydrate transport & metabolism
Lignin peroxidase	Carbohydrate transport & metabolism
Metallo-dependent hydrolase	Carbohydrate transport & metabolism
Glycoside hydrolase family 3 protein	Carbohydrate transport & metabolism
PAH-inducible cytochrome P450 monooxygenase	Carbohydrate transport & metabolism
Endo-polygalacturonase PG1 (GH28)	Carbohydrate transport & metabolism
Galactose mutarotase-like protein	Carbohydrate transport & metabolism
Hexokinase	Carbohydrate transport & metabolism
Glycoside hydrolase family 27 protein	Carbohydrate transport & metabolism
Phosphopyruvate hydratase/enolase	Carbohydrate transport & metabolism
FMN-linked oxidoreductase	Co-enzyme transport & metabolism
Pyranose 2-oxidase	Co-enzyme transport & metabolism
Acetyl-CoA synthetase-like protein	Co-enzyme transport & metabolism
Mitochondrial carrier protein	Energy production & conversion
UDP-Glycosyltransferase/glycogen phosphorylase	Energy production & conversion
Ca-transporting ATPase	Inorganic ion transport & metabolism
Ctr-domain protein	Inorganic ion transport & metabolism
Hydroxymethylglutaryl-CoA synthase	Lipid transport & metabolism
Cytochrome P450	Secondary metabolites biosynthesis, transport & catabolism
Information storage & processing	
DNase I-like protein	Replication, recombination & repair
DNA ligase 4	Replication, recombination & repair
Not1-domain protein	Transcription
60S ribosomal protein L27a	Translation, ribosomal structure and biogenesis
Cellular process & signalling	
PX-domain protein	Intracellular trafficking, secretion, and vesicular transport
Sec1-like protein	Intracellular trafficking, secretion, and vesicular transport
Metal resistance protein YCF1	Intracellular trafficking, secretion, and vesicular transport
Acid protease	Posttranslational modification, protein turnover, chaperones
CDK-activating kinase assembly factor	Posttranslational modification, protein turnover, chaperones
Phosphotyrosyl phosphatase activator	Signal transduction mechanisms
Undefined kinase	Signal transduction mechanisms
Kinase-like protein	Signal transduction mechanisms

replaced *T. versicolor*, than in blocks where *H. fasciculare* was not interacting with *T. versicolor*. Hiscox et al. (2015) measured greater CO_2 evolution as a proxy for increased metabolic activity in beech wood blocks where *T. versicolor* interacted with *H. fasciculare*, compared with single species only control blocks. Mixed species communities may cause increased decomposition rates through resource partitioning (Nielsen et al., 2011), i.e. species target different substrate polymers as part of their nutrition, leading to a greater loss of substrate integrity and mass when compared to single species systems. Competitive interactions between wood decay fungi have also been associated with increased oxidative enzyme activity, including peroxidases and laccases also associated with substrate depolymerisation (Baldrian, 2004; Hiscox et al., 2010a), which may enhance decay of the wood block. It is also possible that translocation of resources by the *H. fasciculare* corded network towards the wood block containing *T. versicolor* may lead to greater exploitation of resources once the competitor was overcome.

4.2. Transcriptome and protein comparisons and general observations

The quantified transcriptomic data allowed the identification of putative transcripts differentially regulated between interaction and single species-only samples. The protein analysis recorded presence or absence without considering relative levels between samples, and it was not possible to determine which species a protein originated from when investigating the interaction samples. There was limited similarity between the two datasets, e.g. ATP synthase F1 alpha subunit from *T. versicolor*, and cytochrome P450 and proteases were represented in both groups. Interestingly, transcripts of a cytoplasmic thioredoxin isoenzyme downregulated in *H. fasciculare* and upregulated in *T. versicolor* was identified in protein extracts from both *H. fasciculare* and *T. versicolor* single species-only controls. Time-dependant differences in regulation of transcription and translation in response to abiotic effects was proposed for similar observations in transcriptomic and proteomic profiles during *Phlebia radiata* wood decay (Kuuskeri et al., 2016). Consequently, direct comparison between the transcriptomic and protein datasets should be interpreted with caution.

The competitive antagonistic interaction response of the two fungi when compared against single species controls identified gene transcripts putatively categorised across a range of cellular functions with a greater proportion upregulated (75% *T. versicolor* and 76% *H. fasciculare*) during antagonism than were downregulated. At the time of study, a well annotated *H. fasciculare* genome was unavailable and transcripts were aligned against the high-quality genome annotation of *H. sublaterium* accessed through the JGI Mycocosm portal. As the *T. versicolor* strain was created from the reference genome used in this study, we expected *T. versicolor*-derived transcripts to align strongly and be easily distinguishable from distantly related *H. fasciculare* transcripts. However, this approach is a limitation of the study, and we acknowledge that some *H. fasciculare* transcripts may not have aligned well against the *H. sublateritium* genome, particularly species-specific genes that, consequently, may not have been identified. Other annotations may also not represent true functional homologs leading to caution when interpreting the data, although, genes with highly conserved function can be more confidently assigned. In all cases, further functional analysis is required to determine precise gene function. The relatively low number of transcripts from the interaction wood blocks that aligned with either genome may also have been impacted by the lack of *H. fasciculare* reference genome. In addition, high levels of oxidative enzymes and nucleases are produced during antagonistic fungal interactions (Hiscox et al., 2010a) which may have affected the quality of the RNA extracted and subsequent alignments, compounded further by the challenges in extracting nucleic acids from solid wood cultures.

Posttranslational modification, protein turnover and chaperones was the most represented KOG category in the transcriptomes of each fungus. Despite differences in the specific transcript profiles, the intracellular processing of proteins, particularly via the ubiquitin-proteosome pathway, appears to be an important response to antagonism for both fungi. The upregulation of ubiquitin activating enzyme transcripts in *T. versicolor-H. fasciculare* competition agar cultures has been recorded previously (Eyre et al., 2010) and the rapid degradation of specific cellular proteins might be expected during dynamic antagonism between fungi.

4.3. The H. fasciculare response: Protein and RNA turnover in response to T. versicolor antagonism and nutrient availability

The *H. fasciculare* transcriptional response to the competitive replacement of *T. versicolor* putatively involved the increased turnover of proteins, RNA processing and turnover, ribosome biosynthesis and the targeting of a range of carbohydrate polymers. A shift in physiology and cellular turnover as the fungus enters the new nutrient resource occupied by *T. versicolor* is supported by the upregulation of transcripts encoding 90S and 60S ribosomal genes suggesting increased protein production (Warner, 1991; Giardina et al., 2012) and transcripts encoding RNAses and enzymes reducing RNA stability (Scheffler et al., 1998; Yang et al., 2023). The gene with the greatest increase in

transcripts was a polyadenylation cleavage factor (22-fold increase) which also suggests increased mRNA processing activity. The upregulation of poorly characterised putative fungal-specific transcription factors and genes regulating the methylation of histones may also provide targets for future research into how the shift in cellular responses are regulated (Lai et al., 2022).

The production of new proteins by *H. fasciculare* during the interaction appears to be linked to the breakdown of existing cellular proteins either through proteinases or ubiquitin-proteasomal pathway transcripts identified in this study. We hypothesise that new proteins are generated from existing intracellular resource and the increased turnover of proteins maybe a consequence of relative nitrogen limitation due to increased carbon input from the newly colonised substrate. The unexpected lack of upregulation of any transcripts associated with amino acid transport in the interaction samples may be because the single species control comparator demonstrated similar nitrogen translocation mechanisms (Boberg et al., 2014; Philpott et al., 2014). Increased transcription of glycoside hydrolase genes targeting cellulose, hemicellulose and pectin compared with the colonisation of single species control wood blocks indicates that *H. fasciculare* has increased access to plant cell wall polymers when replacing *T. versicolor*. As a strongly ligninolytic white rot decay species, *T. versicolor* could have disrupted the lignified cell wall components of the wood block more than the *H. fasciculare* control providing greater access to the sugar-based polymers, supporting a resource partitioning hypothesis (Nielsen et al., 2011) and causing the greater loss of mass recorded in the competitive interaction blocks. Interestingly, no transcripts associated with energy production were upregulated by *H. fasciculare* while three enzymes putatively associated with cell cycle progression were. This could suggest that resource acquisition and intracellular macromolecule turnover in the *H. fasciculare* antagonism is associated with increased biomass production rather than increased respiration or energy generation often described for antagonistic fungal interactions (Hiscox et al., 2015). Increased biomass and territorial occupation has been recorded as an important determinant in successful replacement strategies in competing fungi (Hiscox et al., 2018).

4.4. The *T. versicolor* response: Increased signalling and metabolic activity with regulation of intracellular nitrogen resource

The *T. versicolor* transcriptomic response to *H. fasciculare* antagonism included putative evidence of targeted protein turnover and amino acid transport, a shift in signal transduction pathways, and increased energy generation and mitochondrial activity. The change in transcript levels of several kinases (three up- and two down-regulated) indicates a shift in signalling activity as the fungus responds to a fundamental change in its environment. It is not possible to identify which signalling pathways these enzymes target as they have broad function in regulating cellular processes and gene expression (Dickman and Yarden 1999; Park et al., 2011). Consideration of these kinases with the up-regulation of two transcription factors, histone deacetylase and downregulation of a cytosine-5-methyltransferase may provide targets for future studies aiming to understand the regulation of interspecific interactions in *T. versicolor*.

In addition to two proteinases, four F-box proteins and a segregase complex-associated AAA ATPAse were upregulated suggests that active protein turnover occurs during the interaction with *H. fasciculare*. While F-box protein function is varied, they are associated with regulating cellular levels of targeted proteins via ubiquitin-mediated degradation, including proteins involved in cell cycle progression, nutrient sensing and mitochondria functioning (Jonkers and Rep, 2009). Further research is required to determine whether the unexpected down-regulation of HECT-type E3 ligase might indicate greater dominance for RING-type E3 ligase reactions in protein processing and degradation (Metzger et al., 2014). Amino acid and lipid transport and metabolism transcripts featured more prominently in *T. versicolor*, where three amino acid permeases/transporters were upregulated. The translocation of amino acids has been associated with resource mobilisation in other fungi (Tlalka et al., 2008; Boberg et al., 2014), their expression may also be linked to the release of amino acids during the degradation of proteins described above. Nitrogen dynamics in the resource-limited *T. versicolor* may be an important factor in regulating transcriptional responses, as previous work measured a reduction in the intracellular ubiquitin pool and activity of the ubiquitin-proteosome pathway in *T. versicolor* caused by nitrogen limitation (Staszczak, 2008). The apparent lack of transcripts associated with the formation of new proteins or biomass suggest that amino acid transport by *T. versicolor* might function to translocate resources away from the interaction front during *H. fasciculare* replacement.

Increased respiration in *T. versicolor* interspecific antagonistic interactions was recorded previously (Hiscox et al., 2015), although the response could not be ascribed directly to *T. versicolor*. Our data identified several transcripts and proteins associated with mitochondrial function and energy generation that could be associated with the observed increase in respiration. Transcripts of components of mitochondrial F1F0 synthase were upregulated in interaction wood blocks, along with transcripts encoding putative COX15-like protein associated with cytochrome *c* complex assembly (Glerum et al., 1997), a mitochondrial ADP/ATP carrier protein and a DUF124 protein linked to the formation of mitochondrial membranes (Hess et al., 2009). *T. versicolor* may, therefore, be the origin of ATP synthase F1 alpha subunit and mitochondrial carrier protein peptides identified in the interaction proteome. The number of dehydrogenase enzymes, including two alcohol dehydrogenases, and hemethryn-like protein associated with oxygen transport with increased transcription also suggests a response to localised reduced oxygen levels (Okamoto et al., 2014; Mattila et al., 2020).

4.5. Putative signatures of direct antagonism response and active secondary metabolic pathways

Direct antagonism between fungal cells is associated with a range of competition-associated responses that weaken the antagonist or exploit its resources (Hiscox and Boddy, 2017). The proteinases produced by both fungi and putative GH18 chitinase transcripts by *H. fasciculare* could be associated with direct antagonism between the species or nutrient acquisition from captured resources (Lindahl and Finlay, 2006; Iqbal et al., 2018). However, GH18 chitinases have also been implicated in cell wall remodelling during active growth (Gruber and Siedl-Seiboth, 2012). The increased transcription of a serpin-like protease inhibitor by *T. versicolor* also indicates a potential role for proteinases during antagonism (Burchacka et al., 2022) and the upregulation of glutathione-S-transferase by *T. versicolor* may also be involved in defence against xenobiotics present in the interspecific interaction (Arfi et al., 2013). Both fungi are known to produce a range of secondary metabolites (Zhang et al., 2020; Al-Salihi et al., 2021) and the role of secondary metabolites in antagonistic interactions has been described (Rangel et al., 2021). The increased transcription of a *T. versicolor* putative isoprenoid synthase gene during the interaction with *H. fasciculare* could be linked to the secondary metabolic response of the fungus. The gene is in a chromosome region with two other isoprenoid synthase genes in the *T. versicolor* genome (Supplementary Fig. S9) and, while the products of the genes are unknown, they are interesting targets for future characterisation. An ortholog of the *T. versicolor* putative phenylpyruvate tautomerase gene has also been implicated in hydroxy-phenylpropanoate secondary metabolite production in plant pathogenic fungi (Cimmino et al., 2018), but similar compounds have yet to be described in *T. versicolor*.

Direct antagonism-related transcripts identified in *H. fasciculare* included a putative non-ribosomal peptide synthase and a protein with conserved berberine/berberine-like domain associated with the biosynthesis of isoquinoline alkaloids and cytochalasins (Facchini et al.,

1996; Zhang et al., 2022). The isoquinoline alkaloid ankorine was identified previously in wood blocks where *T. versicolor* had been replaced by *H. fasciculare* (O'Leary et al., 2021). Interestingly, the presence of a hydroxymethylglutaryl-Co-A synthase in all proteomic samples and the relatively high abundance of acetyl Co-A synthase peptides in the interaction wood blocks may indicate general activity of the mevalonate-dependant isoprenoid biosynthesis pathway during the antagonistic interaction (Miziorko, 2011). The genes and proteins identified in this study should be targeted for further functional characterisation to determine their role in interspecific interactions.

5. Conclusions

The transcriptomic and proteomic profiling of the antagonistic replacement of *T. versicolor* by a foraging colony of *H. fasciculare* provides an ecologically-relevant interaction scenario not investigated previously, namely the transition between a secondary resource-limited decay species and a late stage, non-resource limited wood decay specialist. Protein turnover and production of new peptides appears to be fundamentally important to both fungi during the antagonism. The *H. fasciculare* response to territory capture highlighted the associated change in RNA and ribosome processing and the importance of the depolymerisation of carbon resources in the substrate. While *T. versicolor* engaged a shift in signalling pathways, energy generation and amino acid transport and metabolism. The enzymes putatively associated with antagonism and secondary metabolite production or detoxification identified for both fungi underline the competitive nature of the interaction between the two species and could direct future research into the discovery of bioactive molecules.

CRediT authorship contribution statement

G. Attrill: Conceptualization, Data curation, Formal analysis, Investigation, Methodology, Writing – original draft. **L. Boddy:** Conceptualization, Funding acquisition, Supervision, Writing – review & editing. **E. Dudley:** Data curation, Formal analysis, Methodology, Supervision, Writing – review & editing. **B. Greenfield:** Data curation, Formal analysis, Writing – review & editing. **D.C. Eastwood:** Conceptualization, Data curation, Formal analysis, Funding acquisition, Investigation, Methodology, Project administration, Supervision, Writing – original draft.

Declaration of competing interest

The authors declare that they have no known competing financial interests or personal relationships that could have appeared to influence the work reported in this paper.

Acknowledgements

The research described in this manuscript was funded by UK Natural Environment Research Council award reference 1319716. We also thank Jennifer Hiscox and Melanie Savory for advice with experimental design.

Appendix A. Supplementary data

Supplementary data to this article can be found online at https://doi.org/10.1016/j.funeco.2024.101385.

References

Al-Salihi, S.A.A., Bull, I.D., Al-Salhi, R., Gates, P.J., Salih Kifah, S.M., Bailey, A.M., Foster, G.D., 2021. Further biochemical profiling of *Hypholoma fasciculare* metabolome reveals its chemogenetic diversity. Front. Bioeng. Biotechnol. 9, 567384. https://doi.org/10.3389/fbioe.2021.567384.

Anders, D., Pyl, P.T., Huber, W., 2015. HTSeq - a Python framework to work with high-throughput sequencing data. Bioinformatics 31 (2), 166–169. https://doi.org/10.1093/bioinformatics/btu638.

Arfi, Y., Levasseur, A., Record, E., 2013. Differential expression in Pycnoporus coccineus during interspecific mycelial interactions with different competitors. Appl. Environ. Microbiol. 79 (21), 6626–6636. https://doi.org/10.1128/AEM.02316-13.

Baldrian, P., 2004. Increase of laccase activity during interspecific interactions of white-rot fungi. FEMS (Fed. Eur. Microbiol. Soc.) Microbiol. Ecol. 50, 245–253. https://doi.org/10.1016/j.femsec.2004.07.005.

Baldrian, P., 2008. Enzymes of saprotrophic basidiomycetes. In: Woodward, S., Boddy, L. (Eds.), Ecology of Saprotrophic Basidiomycetes. Academic Press, Oxford, pp. 19–41. https://doi.org/10.1016/S0275-0287(08)80004-5.

Ballasen, V., Luyssaert, S., 2014. Carbon sequestration: managing forests in uncertain times. Nature 596 (7487), 153–155. https://doi.org/10.1038/506153a.

Benjamini, Y., Hochberg, Y., 1995. Controlling the false discovery rate: a practical and powerful approach to multiple testing. J. Roy. Stat. Soc. B 57, 289–300. https://doi.org/10.1111/j.2517-6161.1995.tb02031.x.

Boberg, J.B., Finlay, R.D., Stenlid, J., Ekblad, A., Lindahl, B.D., 2014. Nitrogen and carbon reallocation in fungal mycelia during decomposition of boreal forest litter. PLoS One 9 (3), e92897. https://doi.org/10.1371/journal.pone.0092897.

Boddy, L., 1999. Saprotrophic cord-forming fungi: meeting the challenge of heterogeneous environments. Mycologia 91, 13–32. https://doi.org/10.1080/00275514.1999.12060990.

Boddy, L., 2000. Interspecific combative interactions between wood-decaying basidiomycetes. FEMS (Fed. Eur. Microbiol. Soc.) Microbiol. Ecol. 31, 185–194. https://doi.org/10.1111/j.1574-6941.2000.tb00683.x.

Boddy, L., 2016. Interactions between fungi and other microbes. In: Watkinson, S.C., Boddy, L., Money, N.P. (Eds.), The Fungi, third ed. Elsevier Inc., Amsterdam, pp. 337–360. https://doi.org/10.1016/B978-0-12-382034-1.00010-4.

Boddy, L., Heilmann-Clausen, J., 2008. Basidiomycete community development in temperate angiosperm wood. In: Boddy, L., Frankland, J.C., van West, P. (Eds.), Ecology of Saprotrophic Basidiomycetes. Elsevier Inc., Amsterdam, pp. 209–235. https://doi.org/10.1016/S0275-0287(08)80016-1.

Boddy, L., Hiscox, J., 2016. Fungal ecology: principles and mechanisms of colonization and competition by saprotrophic fungi. Microbiol. Spectr. 4 (6). https://doi.org/10.1128/microbiolspec.FUNK-0019-201.

Boddy, L., Watkinson, S.C., 1995. Wood decomposition, higher fungi, and their role in nutrient redistribution. Can. J. Bot. 73, 1377–1383. https://doi.org/10.1139/b95-400.

Bradford, M., 1976. A rapid and sensitive method for the quantification of microgram quantities of protein utilizing the principle of protein-dye binding. Anal. Biochem. 72 (1–2), 248–254. https://doi.org/10.1006/abio.1976.9999.

Burchacka, E., Pięta, P., Łupicka-Słowik, A., 2022. Recent advances in fungal serine protease inhibitors. Biomed. Pharmacother. 146, 112523. https://doi.org/10.1016/j.biopha.2021.112523.

Chase, J.M., 2003. Community assembly: when should history matter? Oecologia 136, 489–498. https://doi.org/10.1007/s00442-003-1311-7.

Cimmino, A., Nocera, P., Linaldeddu, B.T., Masi, M., Gorecki, M., Pescitelli, G., Montecchio, L., Maddau, L., Evidente, A., 2018. J. Agric. Food Chem. 66 (13), 3435–3442. https://doi.org/10.1021/acs.jafc.8b00256.

Crowther, T.W., Boddy, L., Jones, T.H., 2011. Species-specific effects of soil fauna on fungal foraging and decomposition. Oecologia 167, 535–545. https://doi.org/10.1007/s00442-011-2005-1.

Dawson-Andoh, B.E., Morrell, J.J., 1992. Extraction of proteins from wood wafers colonized by decay fungi. Holzforschung 46 (2), 117–120. https://doi.org/10.1515/hfsg.1992.46.2.117.

Dickman, M.B., Yarden, O., 1999. Serine/threonine protein kinases and phosphatases in filamentous fungi. Fungal Genet. Biol. 26 (2), 99–117. https://doi.org/10.1006/fgbi.1999.1118.

Evans, J.A., Eyre, C.A., Rogers, H.J., Boddy, L., Müller, C.T., 2008. Volatile production during interspecific interactions between *Trametes versicolor, Stereum gausapatum, Hypholoma fasciculare* and *Bjerkandera adusta* in culture. Fungal Ecology 1, 57–68. https://doi.org/10.1016/j.funeco.2008.06.001.

Eyre, C., Muftah, W., Hiscox, J., Hunt, J., Kille, P., Boddy, L., Rogers, H.J., 2010. Microarray analysis of differential gene expression elicited in *Trametes versicolor* during interspecific mycelial interactions. Fungal Biol. 114, 646–660. https://doi.org/10.1016/j.funbio.2010.05.006.

Facchini, P.J., Penzes, C., Johnson, A.G., Bull, D., 1996. Molecular characterization of berberine bridge enzyme genes from opium poppy. Plant Physiol. 112 (4), 1669–1677. https://doi.org/10.1104/pp.112.4.1669.

Fawcett, R.G., Collis-George, N., 1967. A filter paper method for determining the moisture characteristic of soil. Aust. J. Exp. Agric. 7, 162–167. https://doi.org/10.1071/EA9670162.

Floudas, D., Binder, M., Riley, R., Barry, K., Blanchette, R.A., Henrissat, B., Martinez, A. T., Otillar, R., Spatafora, J.W., Yadav, J.S., Aerts, A., Benoit, I., Boyd, A., Carlson, A., Copeland, A., Coutinho, P.M., de Vries, R.P., Ferreira, P., Findley, K., Foster, B., Gaskell, J., Glotzer, D., Gorecki, P., Heitman, J., Hesse, C., Hori, C., Igarashi, K., Jurgens, J.A., Kallen, N., Kersten, P., Kohler, A., Kues, U., Kumar, T.K., Kuo, A., LaButti, K., Larrondo, L.F., Lindquist, E., Ling, A., Lombard, V., Lucas, S., Lundell, T., Martin, R., McLaughlin, D.J., Morgenstern, I., Morin, E., Murat, C., Nagy, L.G., Nolan, M., Ohm, R.A., Patyshakuliyeva, A., 2012. The Paleozoic origin of enzymatic lignin decomposition reconstructed from 31 fungal genomes. Science 336, 1715–1719. https://doi.org/10.1126/science.1221748. PMID: 22745431.

Fricker, M.D., Lee, J.A., Bebber, D.P., Tlalka, M., Hynes, J., Darrah, P.R., Watkinson, S.C., Boddy, L., 2008. Imaging complex nutrient dynamics in mycelial networks. J. Microsc. 231 (2), 317–331. https://doi.org/10.1111/j.1365-2818.2008.02043.x.

Fricker, M.D., Heaton, L.L.M., Jones, N.S., Boddy, L., 2017. The mycelium as a network. Microbiol. Spectr. 5, 3. https://doi.org/10.1128/microbiolspec.FUNK-0033-2017.
Gessner, M.O., Swan, C.M., Dang, C.K., McKie, B.G., Bardgett, R.D., Wall, D.H., Hättenschwiler, S., 2010. Diversity meets decomposition. Trends Ecol. Evol. 25, 372–380. https://doi.org/10.1016/j.tree.2010.01.010.
Giardina, B.J., Stanley, B.A., Chiang, H.L., 2012. Comparative proteomic analysis of transition of *saccharomyces cerevisiae* from glucose-deficient medium to glucose-rich medium. Proteome Sci. 10, 40. https://doi.org/10.1186/1477-5956-10-40.
Glaus, P., Honkela, A., Rattray, M., 2012. Identifying differentially expressed genes from RNA-seq data with biological variation. Bioinformatics 28 (13), 1721–1728. https://doi.org/10.1093/bioinformatics/bts260.
Glerum, D.M., Muroff, I., Jin, C., Tzagoloff, A., 1997. COX15 codes for a mitochondrial protein essential for the assembly of yeast cytochrome oxidase. J. Biol. Chem. 272 (30), 19088–19094. https://doi.org/10.1074/jbc.272.30.19088.
Gruber, S., Siedl-Seiboth, V., 2012. Self versus non-self: fungal cell wall degradation in Trichoderma. Microbiology (Reading) 158 (1), 26–34. https://doi.org/10.1099/mic.0.052613-0.
Hess, D.C., Myers, C.L., Huttenhower, C., Hibbs, M.A., Hayes, A.P., Paw, J., Clore, J.J., Mendoza, R.M., San Luis, B., Nislow, C., Giaever, G., Costanzo, M., Troyanskaya, O. G., Caudy, A.A., 2009. Computationally driven, quantitative experiments discover genes required for mitochondrial biogenesis. PLoS Genet. 5 (3), e1000407. https://doi.org/10.1371/journal.pgen.1000407.
Hiscox, J., Boddy, L., 2016. Fungal ecology: principles and mechanisms of colonisation by saprotrophic fungi. Microbiol. Spectr. 4 (6). https://doi.org/10.1128/microbiolspec.FUNK-0019-2016. FUNK-0019-2016.
Hiscox, J., Boddy, L., 2017. Armed and dangerous – chemical warfare in wood decay communities. Fungal Biol. Rev. 31 (4), 169–184. https://doi.org/10.1016/j.fbr.2017.07.001.
Hiscox, J., Baldrian, P., Rogers, H.J., Boddy, L., 2010a. Changes in oxidative enzyme activity during interspecific mycelial interactions involving the white-rot fungus *Trametes versicolor*. Fungal Genet. Biol. 47, 562–571. https://doi.org/10.1016/j.fgb.2010.03.007.
Hiscox, J., Hibbert, C., Rogers, H.J., Boddy, L., 2010b. Monokaryons and dikaryons of *Trametes versicolor* have similar combative, enzyme and decay ability. Fungal Ecology 3 (4), 347–356. https://doi.org/10.1016/j.funeco.2010.02.003.
Hiscox, J., Savoury, M., Vaughan, I.P., Müller, C.T., Boddy, L., 2015. Antagonistic fungal interactions influence carbon dioxide evolution from decomposing wood. Fungal Ecology 14, 24–32. https://doi.org/10.1016/j.funeco.2014.11.001.
Hiscox, J., O'Leary, J., Boddy, L., 2018. Fungus wars: basidiomycete battles in wood decay. Stud. Mycol. 89, 117–124. https://doi.org/10.1016/j.simyco.2018.02.003.
Holmer, L., Renvall, P., Stenlid, J., 1997. Selective replacement between species of wood-rotting basidiomycetes, a laboratory study. Mycol. Res. 101, 714–720. https://doi.org/10.1017/S0953756296003243.
Hori, C., Gaskell, J., Cullen, D., Sabat, G., Stewart, P.E., Lail, K., Peng, Y., Barry, K., Grigoriev, I.V., Kohler, A., Fauchery, L., Martin, F., Zeiner, C.A., Bhatnagar, J.M., 2018. Multi-omic analyses of extensively decayed *Pinus contorta* reveal expression of a diverse array of lignocellulose-degrading enzymes. Appl. Environ. Microbiol. 84 (20), e0113318. https://doi.org/10.1128/AEM.01133-18.
Hynes, J., Müller, C.T., Jones, T.H., Boddy, L., 2007. Changes in volatile production during the course of fungal mycelial interactions between *Hypholoma fasciculare* and *Resinicium bicolor*. J. Chem. Ecol. 33 (1), 43–57. https://doi.org/10.1007/s10886-006-9209-6.
Iqbal, M., Dubey, M., Gudmundsson, M., Viketoft, M., Funck Jensen, D., Karlsson, M., 2018. Comparative evolutionary histories of fungal proteases reveal gene gains in the mycoparasitic and nematode-parasitic fungus *Clonostachys rosea*. BMC Evol. Biol. 18, 171. https://doi.org/10.1186/s12862-018-1291-1.
Jonkers, W., Rep, M., 2009. Lessons from fungal F-box proteins. Eukaryot. Cell 8 (5), 677–695. https://doi.org/10.1128/EC.00386-08.
Kim, D., Pertea, G., Trapnell, C., Pimentel, H., Kelley, R., Salzberg, S.L., 2013. TopHat2: accurate alignment of genomes in the presence of insertions, deletions and gene fusions. Genome Biol. 14, R36. https://doi.org/10.1186/gb-2013-14-4-r36.
Kim, D., Langmead, B., Salzberg, S.L., 2015. HISAT: a fast spliced aligner with low memory requirements. Nat. Methods 12 (4), 357–360. https://doi.org/10.1038/nmeth.3317.
Kuuskeri, J., Häkkinen, M., Laine, P., Smolander, O.-P., Tamene, F., Miettinen, S., Nousiainen, P., Kemell, M., Auvinen, P., Lundell, T., 2016. Time-scale dynamics of proteome and transcriptome of the white-rot fungus *Phlebia radiata*: growth on spruce wood and decay effect on lignocellulose. Biotecnhology for Biofuels. 9, 192. https://doi.org/10.1186/s13068-016-0608-9.
Lai, Y., Wang, L., Zheng, W., Wang, S., 2022. Regulatory roles of histone modifications in filamentous fungal pathogens. Journal of Fungi 8 (6), 565. https://doi.org/10.3390/jof8060565.
Langmead, B., Saltzberg, S.L., 2012. Fast gapped-read alignment with Bowtie 2. Nat. Methods 9, 357–359. https://doi.org/10.1038/nmeth.1923.
Lindahl, B.D., Finlay, R.D., 2006. Activities of chitinolytic enzymes during primary and secondary colonization of wood by basidiomycetous fungi. New Phytol. 169, 389397. https://doi.org/10.1111/j.1469-8137.2005.01581.x.
Martin, M., 2011. Cutadapt removes adapter sequences from high-throughput sequencing reads. EMBnet. Journal. 17, 10–12. https://doi.org/10.14806/ej.17.1.200.
Mattila, H.K., Mäkinen, M., Lundell, T., 2020. Hypoxia is regulating enzymatic wood decomposition and intracellular carbohydrate metabolism in filamentous white rot fungus. Biotechnol. Biofuels 13, 26. https://doi.org/10.1186/s13068-020-01677-0.
Metzger, M.B., Pruneda, J.N., Klevit, R.E., Weissman, A.M., 2014. Ring-type E3 ligases: master manipulators of E2 ubiquitin-conjugating enzymes and ubiquitination. Biochim. Biophys. Acta 1834 (1), 47–60. https://doi.org/10.1016/j.bbamcr.2013.05.026.
Miyauchi, S., Navarro, D., Grigoriev, I.V., Lipzen, A., Riley, R., Chevret, D., Grisel, S., Berrin, J.-G., Henrissat, B., Rosso, M.-N., 2016. Visual comparative omics of fungi for plant biomass deconstruction. Front. Microbiol. 7, 1335. https://doi.org/10.3389/fmicb.2016.01335.
Miziorko, H.M., 2011. Enzymes of the mevalonate pathway of isoprenoid biosynthesis. Arch. Biochem. Biophys. 505 (2), 131–143. https://doi.org/10.1016/j.abb.2010.09.028.
Moody, S.C., Dudley, E., Hiscox, J., Boddy, L., Eastwood, D.C., 2018. Interdependence of primary metabolism and xenobiotic mitigation characterizes the proteome of *Bjerkandera adusta* during wood decomposition. Appl. Environ. Microbiol. 84 (2), e01401. https://doi.org/10.1128/AEM.01401-17, 17.
Nelder, J.A., Wedderburn, R.W.N., 1972. Generalized linear models. J. Roy. Stat. Soc. 135, 370–384. https://doi.org/10.2307/2344614.
Nielsen, U.N., Ayres, E., Wall, D.H., Bardgett, R.D., 2011. Soil biodiversity and carbon cycling: a review and synthesis of studies examining diversity-function relationships. Eur. J. Soil Sci. 62, 105–116. https://doi.org/10.1111/j.1365-2389.2010.01314.x.
O'Leary, J., Hiscox, J., Eastwood, D.C., Savoury, M., Langley, A., McDowell, S.W., Rogers, H.J., Boddy, L., Müller, C.T., 2019. The whiff of decay: linking volatile production and extracellular enzymes to outcomes of fungal interactions at different temperatures. Fungal Ecology 39, 336–348. https://doi.org/10.1016/j.funeco.2019.03.006.
Okamoto, K., Uchii, A., Kanawaku, R., Yanase, H., 2014. Bioconversion of xylose, hexoses and biomass to ethanol by a new isolate of the white rot basidiomycete *Trametes versicolor*. SpringerPlus 3, 121. https://doi.org/10.1186/2193-1801-3-121.
O'Leary, J., Journeaux, K.L., Houthuijs, K., Engel, J., Sommer, U., Viant, M.R., Eastwood, D.C., Müller, C., Boddy, L., 2021. Space and patchiness affects diversity–function relationships in fungal decay communities. ISME J. 15, 720–731. https://doi.org/10.1038/s41396-020-00808-7, 2021.
Park, G., Servin, J.A., Turner, G.E., Altamirano, L., Colot, H.V., Collopy, P., Litvinkova, L., Li, L., Jones, C.A., Diala, F.G., Dunlap, J.C., Borkovich, K.A., 2011. Global analysis of serine-threonine protein kinase genes in *Neurospora crassa*. Eukaryot. Cell 10 (11), 1553–1564. https://doi.org/10.1128/EC.05140-11.
Peng, M., Aguilar-Pontes, M.V., Hainaut, M., Henrissat, B., Hilden, K., Mäkelä, M.R., de Vries, R.P., 2018. Comparative analysis of basidiomycete transcriptomes reveals a core set of expressed genes encoding plant biomass degrading enzymes. Fungal Genet. Biol. 112, 40–46. https://doi.org/10.1016/j.fgb.2017.08.001.
Philpott, T.J., Prescott, C.E., Chapman, W.K., Grayston, S.J., 2014. Nitrogen translocation and accumulation by a cord-forming fungus (*Hypholoma fasciculare*) into simulated woody debris. For. Ecol. Manag. 315, 121–128. https://doi.org/10.1016/j.foreco.2013.12.034.
Presley, G.N., Schilling, J.S., 2017. Distinct Growth and secretome strategies for two taxonomically divergent brown rot fungi. Appl. Environ. Microbiol. 83 (7), e02987. https://doi.org/10.1128/AEM.02987-16, 16.
Rangel, L.I., Hamilton, O., de Jonge, R., Bolton, M.D., 2021. Fungal social influencers: secondary metabolites as a platform for shaping the plant-associated community. Plant J. 108 (3), 632–645. https://doi.org/10.1111/tpj.15490.
Rayner, A.D.M., Boddy, L., 1988. Fungal Decomposition of Wood: its Biology and Ecology. Wiley, Chichester.
Reyes, F., Villanueva, P., Alfonso, C., 1990. Comparative study of acid and alkaline phosphatase during the autolysis of filamentous fungi. Lett. Appl. Microbiol. 10, 175–177. https://doi.org/10.1111/j.1472-765X.1990.tb00108.x.
Robinson, M.D., McCarthy, D.J., Smyth, G.K., 2010. edgeR: a Bioconductor package for differential expression analysis of digital gene expression data. Bioinformatics 26, 139–140. https://doi.org/10.1093/bioinformatics/btp616.
Sahu, N., Merényi, Z., Bálint, B., Kiss, B., Sipos, G., Owens, R., Nagy, L.G., 2020. Hallmarks of basidiomycete soft- and white-rot in wood decay -omics data of Armillaria. Microorganisms 9 (1), 149. https://doi.org/10.3390/microorganisms9010149.
Scheffler, I.E., de la Cruz, B.J., Prieto, S., 1998. Control of mRNA turnover as a mechanism of glucose repression in *Saccharomyces cerevisiae*. Int. J. Biochem. Cell Biol. 30 (11), 1175–1193. https://doi.org/10.1016/S1357-2725(98)00086-7.
Staszczak, M., 2008. The role of the ubiquitin–proteasome system in the response of the ligninolytic fungus *Trametes versicolor* to nitrogen deprivation. Fungal Genet. Biol. 45 (3), 328–337. https://doi.org/10.1016/j.fgb.2007.10.017.
Tlalka, M., Fricker, M., Watkinson, S., 2008. Imaging and long-distance α-aminoisobutyric acid translocation dynamics during resource capture by *Serpula lacrymans*. Appl. Environ. Microbiol. 74 (9), 2700–2708. https://doi.org/10.1128/AEM.02765-07.
Tláskal, V., Brabcová, V., Větrovský, T., Jomura, M., López-Mondéjar, R., Oliveira Monteiro, L.M., Saraiva, J.P., Human, Z.R., Cajthaml, T., Nunes da Rocha, U., Baldrian, P., 2021. Complementary roles of wood-inhabiting fungi and bacteria facilitate deadwood decomposition. mSystems 6 (1). https://doi.org/10.1128/msystems.01078-20.
Tordoff, G.M., Boddy, L., Jones, T.H., 2008. Species-specific impacts of collembola grazing on fungal foraging ecology. Soil Biol. Biochem. 40, 434–442. https://doi.org/10.1016/j.soilbio.2007.09.006.
Tornberg, K., Olsson, S., 2002. Detection of hydroxyl radicals produced by wood-decomposing fungi. FEMS (Fed. Eur. Microbiol. Soc.) Microbiol. Ecol. 40, 13–20. https://doi.org/10.1111/j.1574-6941.2002.tb00931.x.
Trapnell, C., Hendrickson, D., Sauvageau, M., Goff, L., Rinn, J., Pachter, L., 2012. Differential analysis of gene regulation at gene resolution with RNA-seq. Nat. Biotechnol. 31, 46–53. https://doi.org/10.1038/nbt.2450.
Warner, J.R., 1991. The economics of ribosome biosynthesis in yeast. Trends Biochem. Sci. 24 (11), 437–440. https://doi.org/10.1016/S0968-0004(99)01460-7.

Wilks, S.S., 1938. The large-sample distribution of the likelihood ratio for testing composite hypotheses. Ann. Math. Stat. 9, 60–62. https://doi.org/10.1214/aoms/1177732360.

Woodward, S., Boddy, L., 2008. Interactions between saprotrophic fungi. In: Boddy, L., Frankland, J.C., van West, P. (Eds.), Ecology of Saprotrophic Basidiomycetes. Academic Press, Oxford, pp. 26–42. https://doi.org/10.1016/S0275-0287(08)80009-4.

Yang, C., Tang, L., Qin, L., Zhong, W., Tang, X., Gong, X., Xie, W., Li, Y., Xia, S., 2023. mRNA turnover protein 4 is vital for fungal pathogenicity and response to oxidative stress in *Sclerotinia sclerotiorum*. Pathogens 12, 281. https://doi.org/10.3390/pathogens12020281.

Zhang, Y., Jingjing Wang, J., Chen Yajun, C., Minghui Zhou, M., Wei Wang, W., Ming Geng, M., Decong Xu, D., Zhongdong Xu, Z., 2020. Comparative genomics uncovers the genetic diversity and synthetic biology of secondary metabolite production of *Trametes*. MYCOBIOLOGY 48 (2), 104–114. https://doi.org/10.1080/12298093.2020.1725361.

Zhang, J.-M., Liu, X., Wei, Q., Ma, C., Li, D., Zou, Y., 2022. Berberine bridge enzyme-like oxidase-catalysed double bond isomerization acts as the pathway switch in cytochalasin synthesis. Nat. Commun. 13, 225. https://doi.org/10.1038/s41467-021-27931-z.